DESIGN OF METHOD FOR CONTROLLING TEMPERATURE IN A CENTRAL SOLAR THERMAL RECEIVER

Claudia Cammarata

Bachelor of Engineering in Mechanical Engineering

Department of Mechanical Engineering
Macquarie University

November 13, 2017

Supervisor: Senior Lecturer Dr. Yijiao Jiang

ACKNOWLEDGMENTS

I would like to acknowledge my academic supervisor Senior Lecturer Dr. Yijiao Jiang for her continual support, guidance and sharing of insightful background knowledge related to this thesis project. I also acknowledge my co-supervisor Research Fellow Dr. Sicong Tian for his encouragement and willingness to exchange ideas, as well assistance with the experimental set-up. Technical officers Wendy Tao and Mynga Nguyen are thanked for their assistance with the prototyping phase of this project, providing access to and assistance with necessary tools and equipment. I am grateful to Professor Candace Lang, Senior Lecturer Shaokoon Cheng and Lecturer Sammy Diasinos from the Mechanical Engineering Department for encouragement and advice provided.

STATEMENT OF CANDIDATE

I, Claudia Cammarata, declare that this report, submitted as part of the requirement for the award of Bachelor of Engineering in the Department of Mechanical Engineering, Macquarie University, is entirely my own work unless otherwise referenced or acknowledged. This document has not been submitted for qualification or assessment at any other academic institution.

Student's Name: Claudia Cammarata

Student's Signature:

Date: 13/11/2017

ABSTRACT

A novel method for controlling the temperature in a central cavity solar receiver has been developed. The solution consists of an aperture control mechanism, altering the size of the window through which solar radiation can enter the receiver. It uniquely utilises the circle-like properties of a squircle to form the aperture, leading to a simple yet effective mechanism with motion facilitated by planetary gears and cam-follower pairs. The design has been validated and illustrated through the use of 3-dimensional computer models and prototype construction. Using analytical and experimental data, it has been demonstrated that this mechanism is able to control temperature in a mock receiver as intended. This has the potential to work with existing concentrated solar thermal (CST) technology to bring an effective source of energy to remote communities as well as make existing processes more efficient. Improvements that can be made with future work such as automation, increased manufacturability and more appropriate materials are also discussed.

Contents

List of Figures

List of Tables

Chapter 1

Introduction

1.1 Statement of Intent

This project was undertaken with the purpose of developing a working design and prototype of a method for controlling the temperature in solar receivers heated using concentrated solar thermal (CST) technology. The chosen method of temperature control was the creation of an aperture control mechanism, able to alter the size of the window through which the solar radiation can enter the receiver. This mechanism has been designed, manufactured and tested, with results demonstrating that the solution is an effective approach to the proposed problem.

1.2 Purpose

The aperture control mechanism can be paired with a solar concentrating parabolic dish and central receiver to form a complete small-scale system able to effectively concentrate available solar energy in the form of heat for numerous applications. The target of the work in the long term is to use the mechanism in the described configuration for local energy harvesting in remote villages or small communities. Its purpose is to facilitate the concentration of heat to be used directly, rather than using the heat to produce electricity. Using concentrated heat from the sun bypasses the need for burning fossil fuels or using electricity to produce heat. Not only does this have environmental benefits such as reduced greenhouse gas emissions, but it also allows for an off-grid energy source, valuable for many communities around the world without easy access to electricity or fuels.

One particularly useful application is water desalination, which requires large amounts of energy [1] and can be vital in regions where freshwater is scarce. Additionally, fuel production can be accomplished through a combination of processes driven by CST technology. Water splitting, where heat rather than electricity is used to drive the process, has been proposed [2]. The H_2O molecules are split to form H_2 (hydrogen) and O_2 (oxy-

gen), where H_2 can be used as a fuel source. Additionally, CO_2 conversion which provides energy-rich CO (carbon monoxide) and O_2 can be achieved. Here, CO can be combined with H_2 to form a large variety of hydrocarbon fuels [3]. In this case, not only is CO_2 not being produced through burning fossil fuels, it is also being taken out of the atmosphere, a double benefit [2]. Many of the above processes have stages that rely on specific temperature ranges to work [4], which is where the temperature control mechanism of this thesis comes in.

The present work is also valuable in allowing the energy harvested using CST technology to be used more effectively with the implementation of temperature control. This is due to improvements in energy conversion efficiency and the ability to control conditions in the receiver regardless of external factors such as weather or time of day. In summary, the aperture control mechanism as described in this report is designed in order to bring useful energy to remote communities as well as address limitations of current CST technology.

1.3 Project Outcomes

An aperture control mechanism has been designed and built which varies the size of the receiver aperture using moving blades or "followers" with a squircle (see Chapter 3) profile. Motion of components is achieved using a planetary gear system with cams and followers. The feasibility of the concept has been validated through engineering design, prototyping and testing, with the mechanism having been manufactured and working as intended. Results from testing provide evidence of the squircle aperture control mechanism's ability to control temperature in a mock receiver.

Whilst it has been shown that varying the aperture size using this mechanism can control temperature in a mock receiver, improvements can be made with future work. More analysis is required in order to determine the exact relationship between aperture area, shape and temperature. This is due to the fact that the geometry of the aperture is variable along with the area as the mechanism moves. In order to achieve finer precision and develop an automatic control system to work with the mechanism, the relationship must be more clearly defined. Better control of testing conditions, more appropriate materials for the mechanism and some simple design changes would also be of value.

Chapter 2

Background

2.1 Concentrated Solar Thermal Technology

2.1.1 Overview

Concentrated solar thermal (CST) technology utilises energy from the sun in the form of heat, hence "thermal" being in the name. This is accomplished through the concentration of the sun's rays by mirrors or lenses (collectors) onto either a linear or point target (receiver) [5]. The receiver, whether it be a tube as with parabolic trough technology (see figure 2.1) or a single unit as with parabolic dish types (figure 2.2), is where the heat is directed and carried by the heat transfer fluid (HTF). The heat can then be used to generate electricity, drive chemical reactions etc. Higher temperatures are typically achieved in CST plants that utilise point rather than linear receiver arrangements due to the large concentration of sunlight being directed onto a single receiver [6]. This thesis is based on designing a temperature control method for use with a central receiver (point target) and a single parabolic dish as the collector.

2.1.2 Central Receiver

In order to understand how temperature in the receiver can be controlled, one must first understand the basics of solar receiver design. Central refers to the position of the receiver relative to the concentrators, having the solar flux directed to a point focus. The two main categories of central receivers are cavity and external [9]. The difference between them is the location of the heat absorbing material. As the names suggest, an external receiver has the absorbing material on the exterior of the receiver, whilst it is within a cavity for a cavity receiver. See figure 2.3 for diagrams of both types.

Large surface area is a major cause of heat loss for external receivers, making reducing the surface area desirable [9]. However, absorbers have maximum operating temperatures and therefore the HTF must be able to carry away the heat faster (higher heat capacity) if the surface area is reduced. Cavity receivers do not suffer from as much convective and

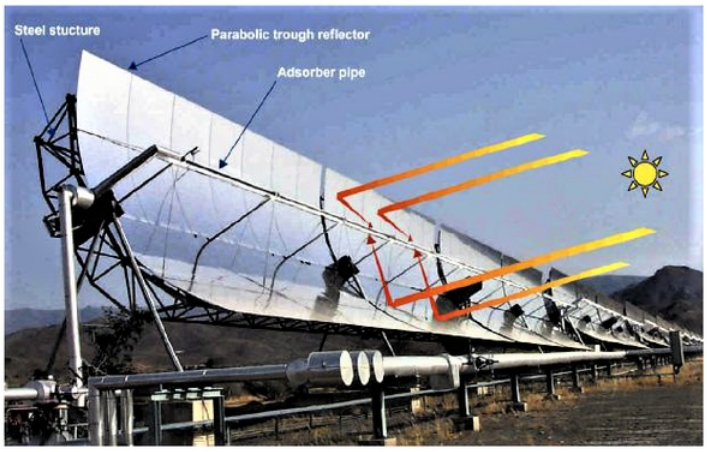

Figure 2.1: Parabolic trough collector with linear tube receiver [7]

Figure 2.2: Parabolic dish collectors with central receivers [8]

radiative heat loss since the absorber lies within a cavity. However, its main drawback is that the solar radiation in contact with the absorber is limited by the acceptance angle of the cavity aperture (60-120° [10]), whereas external absorbers can be targeted from any angle. Since this work is based on a small-scale unit with a single collector, a cavity type with one aperture is the receiver on which the temperature control method is based.

A basic description of a cavity receiver is that it has a cavity where chemical reactions occur, an aperture to let the concentrated light enter, and inlet and outlet ports for feed gas and reaction by-products respectively [11]. See figure 2.4 for a diagram of this. There

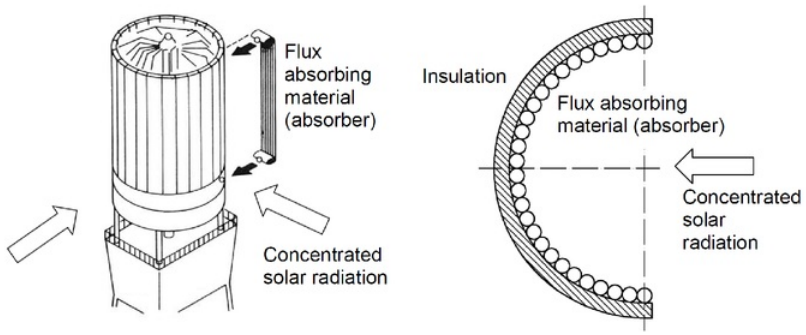

Figure 2.3: External (left) and cavity (right) solar receiver diagrams [10]

are multiple types of cavity receivers, for example; tube, volumetric and solid particle. However, describing them is beyond the scope of this report since the internal workings of the receiver do not affect the design of the external aperture mechanism.

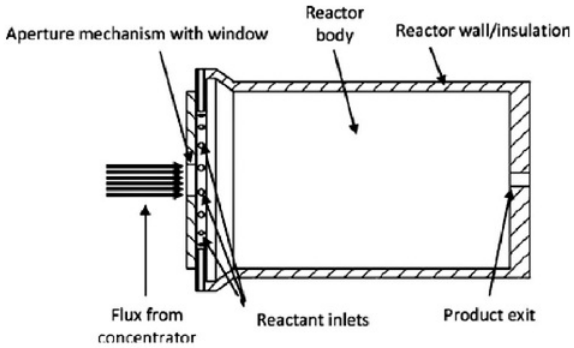

Figure 2.4: Simple cavity receiver schematic with aperture [12]

2.1.3 Heat Concentration

As stated in section 2.1.1, this project is based on controlling the temperature of a cavity receiver with a single parabolic dish concentrator. A parabolic dish focuses incident solar radiation to a point and directs it onto a receiver. See figure 2.5 for a simple representation of this. However, this "point" is actually a circular area with a heat distribution such that the highest temperature is at the centre, cooling down moving outwards [12–15]. This can be seen in figures 2.5 and 2.6, where the heat distribution is represented in terms of concentration ratio and incident flux respectively. This information is valuable as it is important to consider how the light, which is the heat source, interacts with the receiver in order to design an appropriate temperature control method.

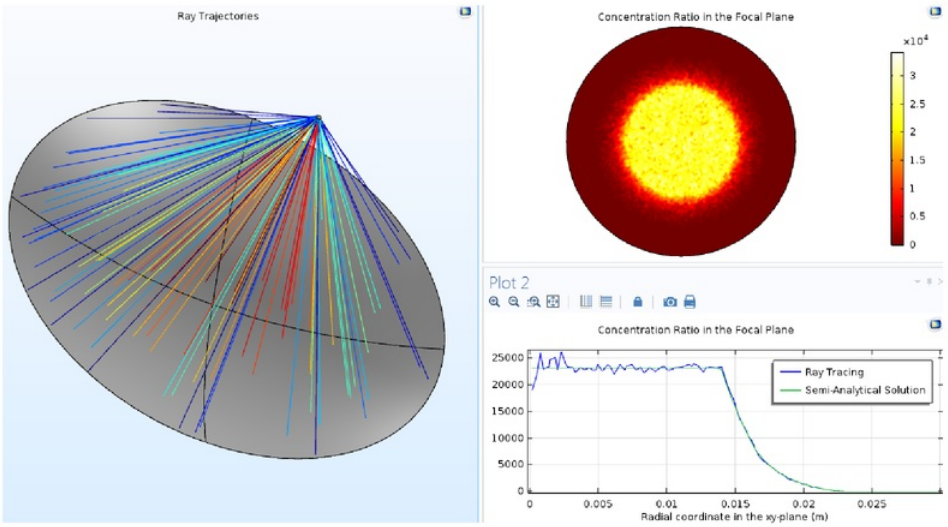

Figure 2.5: Reflected light trajectories (left), concentration ratio distribution in the focal plane (top right), concentration ratio as a function of radial position (bottom right) [13]

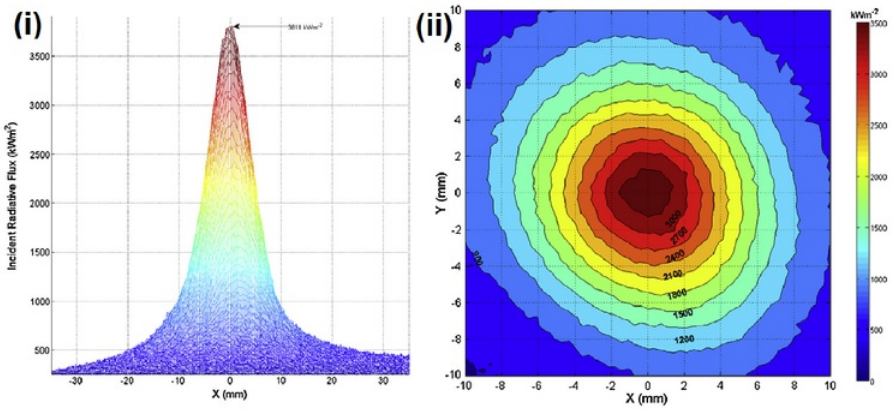

Figure 2.6: Peak flux and Gaussian distribution (i) and spatial flux distribution (ii) of incident flux at the focal plane [15]

2.2 Temperature Control

2.2.1 Purpose

In the context of solar thermochemical conversion (STC), controlling the temperature in a solar receiver could lead to higher efficiency in converting solar to chemical energy. Applying basic thermodynamic principles, one might think having the highest maximum temperature (T_H) is best to promote heat transfer to the absorber due to increased temperature difference. However, a higher T_H also leads to increased heat loss due to re-radiation [2]. There is a $T_{optimum}$ at which these conflicting factors balance to achieve the highest energy transfer efficiency, which varies based on conditions. Being able to change the temperature to consistently achieve the highest possible efficiency would be a great asset to any solar thermochemical process.

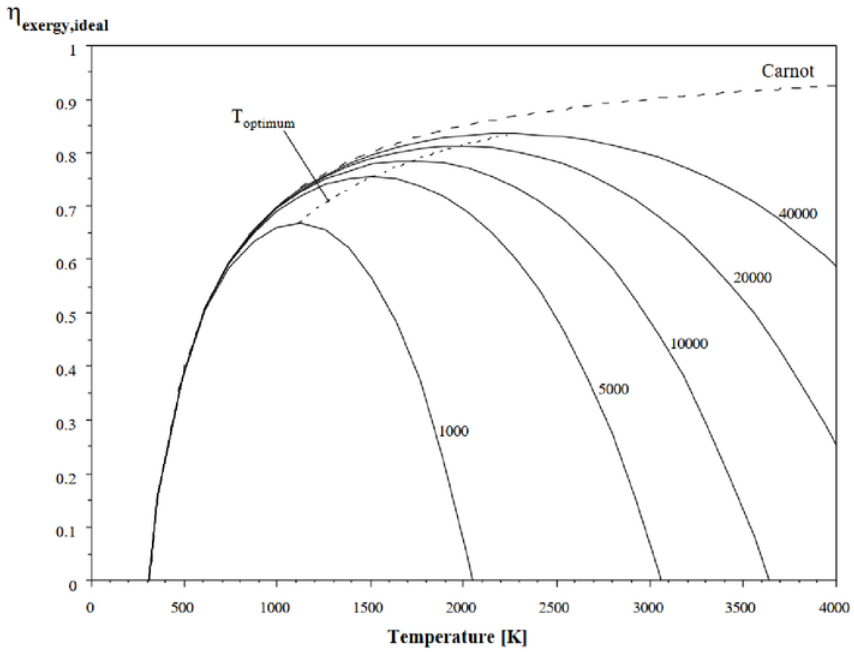

Figure 2.7: Ideal solar-to-fuel energy conversion efficiency to operating temperature T_H (K) for a blackbody cavity receiver converting concentrated solar energy into chemical energy. $T_{optimum}$ is shown for maximum $\eta_{solar-to-fuel,ideal}$ [16]

If a constant temperature in the receiver is desired, the transient nature of solar energy availability due to time of day, weather and so forth is a barrier to achieving this [9]. Thus constant temperature despite external factors can only be achieved through some means

of bypassing these conditions. Another reason why this would be desired is that many chemical reactions can only occur effectively under specific temperatures. Further, a single process can have multiple steps that require different temperatures, for example splitting CO_2 into CO and O_2 [17]. This means that effective control of temperature can make such reactions run more effectively and allow for more complex processes.

2.2.2 Summary of Methods

In order to demonstrate how the decision to base the temperature control method on an aperture control mechanism came about, a brief summary of the main documented techniques is provided here.

Flow Rate

The most widely used method of compensating for solar fluctuations, allowing for temperature to be controlled, is the adjustment of feed gas flow rate [18]. Feed gas is the gas carrying the unreacted chemicals (together or separated) before any conversion processes have occurred. In a direct catalytic absorption receiver (DCAR), which has been used in CO_2 reforming of methane (CH_4), receiver temperature and energy loss are dependent on available solar radiation as well as feed gas flow rate [19]. Since the feed gas carries heat, by increasing its flow rate, more heat is brought to the next stage of the reaction process over the same time period.

In the Catalytically Enhanced Solar Absorption Receiver (CAESAR) project, it was proposed that tailoring of the distribution of feed gas flow may have led to the observed increase in absorber performance [19]. Flow controllers have been used with heat pipe receivers as well [20]. The feed flow rate could be kept constant or controlled automatically depending on solar flux variations to control the temperature [20].

Collector Position

Another method is manipulating the position of the collectors. With solar tower CST plants, a single tall tower holding a receiver is surrounded by a field of heliostats (mirrors with two axis tracking) that concentrate solar energy onto the receiver [8]. Since they collect the solar energy, they have the greatest controllable impact on the heat at the receiver.

By changing the position of a heliostat, one can alter where the solar energy it collects is being directed, or have it not collect any energy at all (facing downwards). In this way, altering the positions of the heliostats can control the temperature at the receiver by compensating for any discrepancies between a chosen reference and a measured temperature [4], by directing more or less light in its direction.

Aperture Size

As incident solar radiation into the receiver increases, so does the receiver's temperature. The aperture is the window through which solar radiation enters the receiver. Thus, it has been reported that both aperture size manipulation and covering have been used as temperature control methods [18, 20, 21] by allowing more or less light to enter. Aperture diameter has an optimum size which depends on the balance between solar exposure and re-radiation losses [21]. Thus being in control of the opening size can assist in achieving this balance by adapting to the conditions. It would also bring about the benefits of temperature control as stated in 2.2.1.

A reduction in temperature can be achieved by blocking the light entering the aperture with some sort of shutter or door of an external housing [20, 21]. Aperture size can also be more directly manipulated through a variable aperture mechanism [18] which varies the size based on the difference between temperature readings and a desired temperature. This was developed in order to reduce the impact of solar radiation fluctuations and allowed for more stable receiver operation than with an uncontrolled system [18].

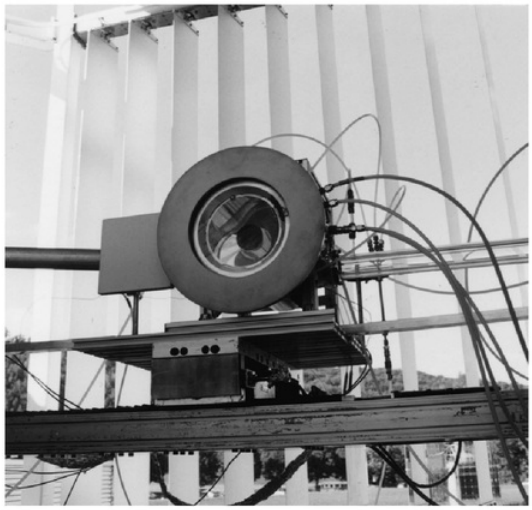

Figure 2.8: Shutters (in the background) used to control the amount of light reaching the receiver [21]

2.3 Variable Aperture

2.3.1 Reasons for Selection

From the options outlined in section 2.2.2, aperture size variation was chosen as the method to be utilised in the design of a temperature control method for a solar receiver, as per the aims of this thesis. The reasons for the selection will be discussed here.

Multiple factors were considered during the selection process. These include appropriateness of the solution to the defined problem, efficacy of the technique and room for further development. Starting with the first consideration, the solution is to be based on the following assumptions:

- The solar receiver is a central cavity type
- The system is small-scale, having one collector (parabolic dish)
- Precise temperature control is desired in the receiver

These assumptions immediately eliminate the collector position option. This is because it is based on the control of the position of heliostats in a solar field, having one receiver atop a tower surrounded by many solar collectors. Though one could argue that a single collector could be controlled in the same way, it would be difficult to achieve precise temperature control as the single aperture is dependent on the single collector moving its focus in minuscule increments. The dish would have to track the sun and have some sort of offset from the ideal position if the temperature was required to be lower.

Next, considering efficacy in achieving precise temperature control, flow rate manipulation and aperture size adjustment were compared. As stated in section 2.2.2, feed gas flow rate manipulation has been the most widely used technique. It has been demonstrated that this method can help achieve greater stability in receiver temperature than that of an uncontrolled system [19, 20, 22].

However, in studies directly comparing aperture size adjustment to feed gas flow rate manipulation for regulating temperature in a solar receiver, aperture control has been found to be the superior method [18, 23]. This is due to more precision in the control and less overshoot of the system (overcompensating for discrepancies between desired and measured temperatures). In the case of a 50% increase in solar radiation, the system controlled via feed gas flow rate manipulation was found to have 3 times greater overshoot than that controlled by aperture size adjustment [18]. Additionally, varying flow rates can disturb the flow dynamics in a receiver, causing problems for processes where constant flow patterns are required [24, 25].

The fact that aperture size adjustment has not been as widely used as a temperature control method as changing feed gas flow rate also made it more likely that the technique

could be developed further or a new mechanism could be designed. Finally, an exterior aperture mechanism does not affect the interior design of a receiver the way a flow variation method likely would, making it easier to isolate the problem from more complex considerations.

2.3.2 Aperture Considerations

Since the temperature control method chosen for this project was aperture adjustment, special attention must be paid to the aperture and how its geometry changes across the transition from open to closed.

Diffraction is the bending of light as it encounters the edge of an object, or in this case, as it passes through the receiver aperture. The light is spread out as the waves encounter the object which creates a pattern dependent on the shape of the aperture. As can be seen in figure 2.9, square and circular apertures exhibit very different diffraction patterns. With a circular aperture, the pattern is known as an Airy pattern. This consists of the bright region in the centre (Airy disc), surrounded by increasingly fainter concentric circular rings moving away from the centre [26].

With a square aperture, there is a bright square-shaped central maximum and four "spikes" made up of increasingly faint rectangular shapes of light radiating outwards. These diffraction spikes are caused by the straight edges of the square aperture. Diffraction spreads out the light waves perpendicular to the straight edge, so a square aperture has 4 spikes and an octagonal aperture would have 8 spikes, for example [27].

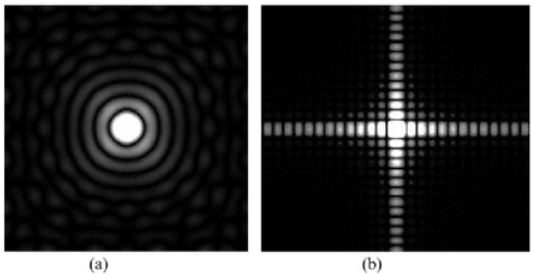

Figure 2.9: Diffraction patterns through (a) circular and (b) square apertures [28]

Since the distribution of light and therefore heat is roughly a circle with its hottest point in the centre (see section 2.1.3), having a circular aperture is ideal as it would overlap with more regions of higher heat concentration than other shapes of the same area. As can be seen in figure 2.10, though a square has regions that extend out further than a circle of the same area, these areas have lower heat concentration and therefore some of the available energy would be sacrificed. Additionally, the diffraction pattern is uniform

about the centre for a circular aperture and therefore allows for more even heat transfer inside the receiver.

It is for those reasons above that in designing the aperture control mechanism of this thesis project, the aim was to maintain an approximately circular aperture for most of the transition between open and closed. This was achieved through the use of the "squircle", which will be explained in more detail in Chapter 3.

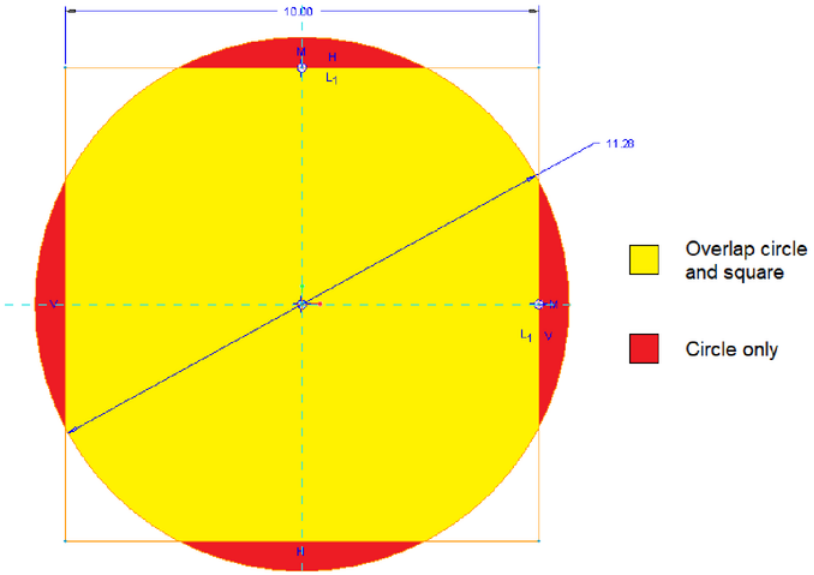

Figure 2.10: Comparing overlapping regions of a square and circle of same area

2.3.3 Previous Work

Early work involving adjusting the amount of light able to enter the receiver through the aperture involved indirect control. One example is the input solar energy being varied via mechanically opening and closing the doors of the building that housed the concentrating mirror [20]. In another similar case, the energy in was controlled using Venetian-like shutters [21]. Both of these studies involved receivers with a fixed aperture size so are dissimilar to the work of this thesis, but paved the way for the development of more direct aperture-based temperature control solutions.

More recently, the focus has been on being able to manipulate the amount of solar energy able to enter the receiver by changing the size of the aperture itself. This has been achieved through the use of both translating (moving in a straight line) or rotating "blades" that overlap and together form the aperture. One early solution is presented in figures 2.11 and 2.12. The solution is mechanically simple in that it utilises only 2 blades driven by a rack and pinion system, attached to a frame (see figure 2.11).

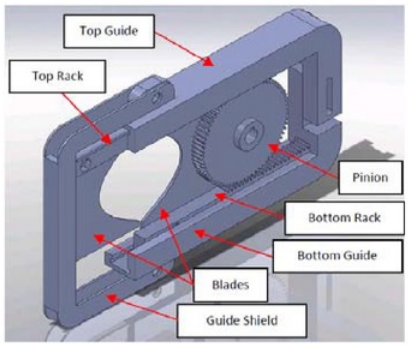

Figure 2.11: 2-bladed rack and pinion mechanism [29]

The main drawback of this design is the increasingly non-circular nature of the aperture shape as it closes (see figure 2.12). Available solar energy is sacrificed in using non-circular apertures [12]. This is due to a number of factors, such as the heat distribution of the concentrated solar energy being circular as described in section 2.1.3, and diffraction effects (see section 2.3.2).

Mechanisms using multiple rotating blades similar to a camera (see figure 2.13) have also been designed. For these types, having more blades leads to a more circular shape. The geometry of the blades (curved versus straight) also influences the aperture shape as it goes from fully open to fully closed [24]. An 8-blade mechanism has been designed, balancing the geometrical advantages of more blades with the potential problems of overall thickness and blade interference if too many are used [24, 30]. Despite using 8 curved

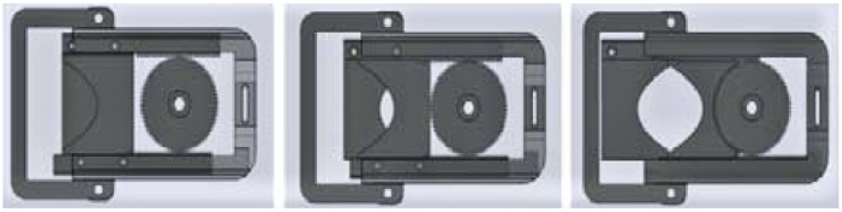

(a) CAD model

(b) Manufactured mechanism

Figure 2.12: CAD model and mechanism as the aperture is opened [12]

blades, the profile still becomes more sharp and octagonal as the aperture closes rather than being a perfect circle [24, 30, 31]. See figure 2.16.

The blades are rotated via a stepper motor coupled to a sprocket which drives the actuator (interface component) using a chain. This actuator is linked to the blades via pins and thus governs their motion. See figure 2.17 for an exploded model of the components described.

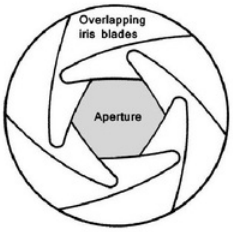

Figure 2.13: Diagram of a typical iris diaphragm for a camera [32]

A more recent solution has incorporated shape memory alloy (SMA) springs instead of motors and chains or bar linkages as described previously, in order to drive the actuator [30]. SMAs are inter-metallic alloys that can change their shape based on temperature. The springs extend or retract based on temperature, driving the mechanism. This eliminates the need for motors which must be cooled constantly and the energy for actuating the mechanism is provided by the heat itself.

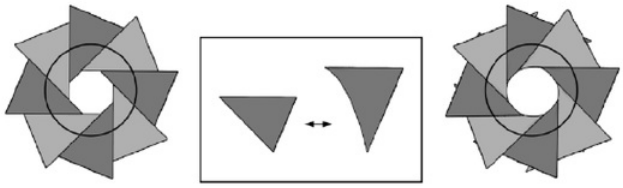

Figure 2.14: 8-blade aperture: straight (left) and curved (right) blades. Curved blades were used to create a more circular profile [24]

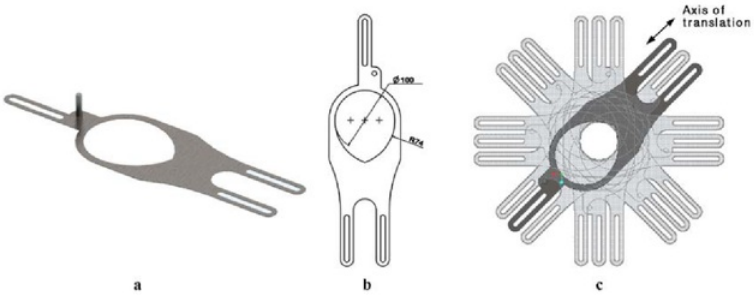

Figure 2.15: Design of blades used in 8-blade iris mechanism [24]

However, some drawbacks include the non-linear variation in force from the spring with increased temperature and the asymmetry between the response time of opening and closing the aperture. It was found that the time to close the aperture was much less than the time to open it. Precision in controlling blade positions was also difficult with this design. Thus further work such as increasing heat transfer to the SMA spring via a heating resistor and a control system is required in order to see the advantages of this concept. See figures 2.19 and 2.20 for visualisation.

The previously described mechanisms were based on maintaining a circular aperture. The following are examples that are similar to the work of this thesis in that they utilise 4 translating components to form the aperture, but have inappropriate aperture shapes for the application based on information provided in sections 2.1.3 and 2.3.2.

Figure 2.22 shows a mechanism using 4 sliding blocks to form the square or rectangular aperture [33]. These blocks are translated via guide rods which are driven by a worm gear and pinions. It is similar to the work of this report in that 4 components form the aperture and these travel linearly rather than rotate to adjust the aperture size. However, the drive mechanism does not involve planetary gears as the present work does and no attempt is made to approximate a circular aperture.

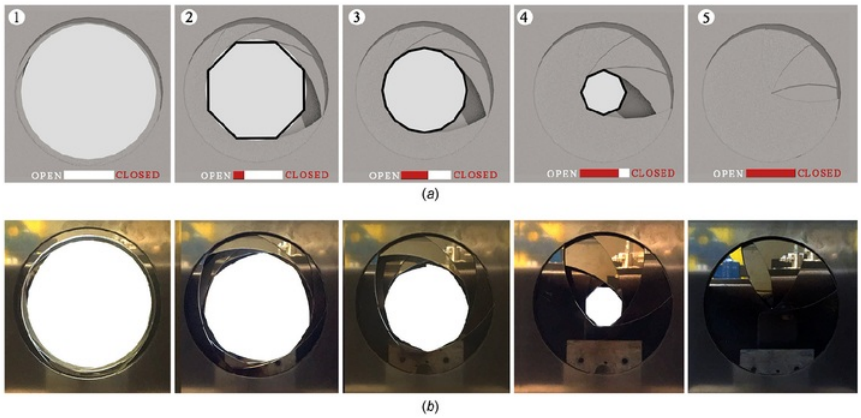

Figure 2.16: Aperture area shape change as it closes - CAD and manufactured [31]

A micro-electromechanical systems (MEMS) variable aperture mechanism has also been fabricated [34]. It works by having 4 shutter blades translate synchronously to form a variable square aperture. Each blade is driven by a separate electro-thermal actuator. These actuators are connected electrically so with an increase in current, temperature rises and the actuators expand linearly.

To summarise, previous work has included mechanisms both within the field of solar concentration and outside of it. Though the work of this thesis has been informed by some of the design considerations of these solutions, it approaches the problem in a unique way that will be demonstrated further into this report.

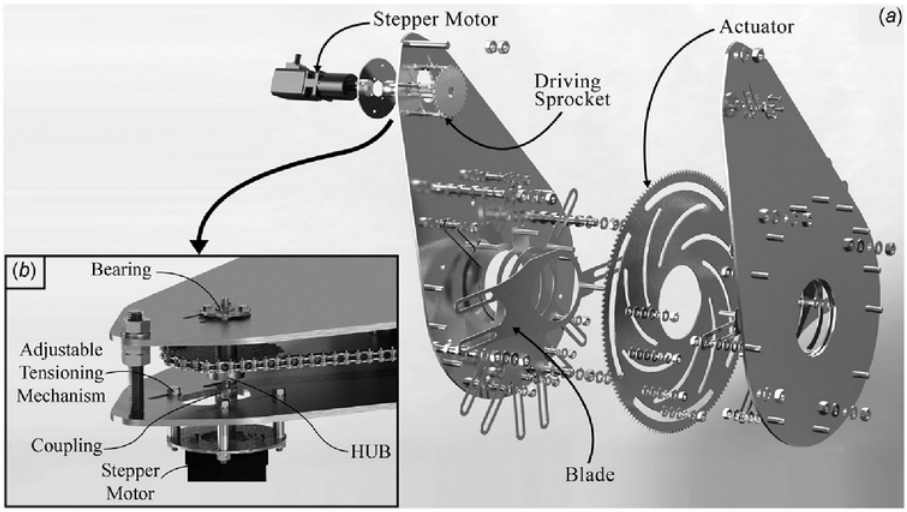

Figure 2.17: Exploded view of complete mechanism [31]

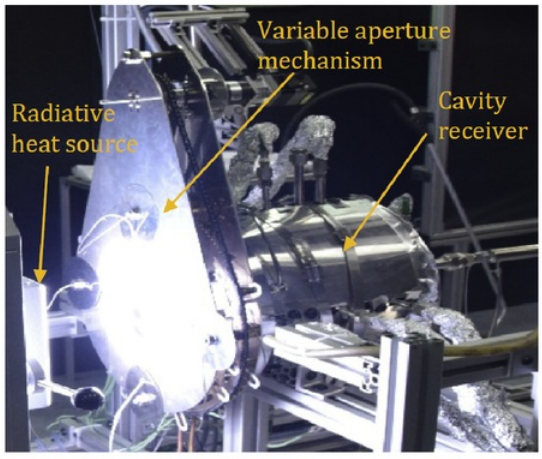

Figure 2.18: Experimental set-up for testing the 8-blade mechanism [18]

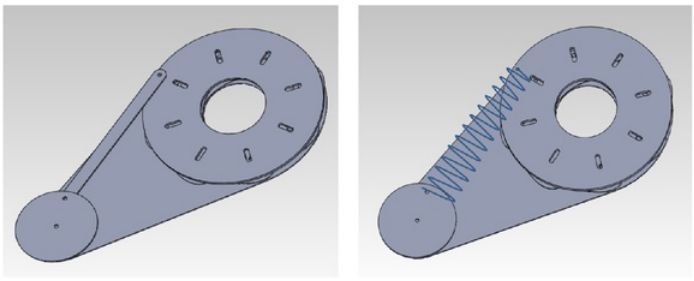

Figure 2.19: Replacing bar linkage with an SMA spring for actuation [30]

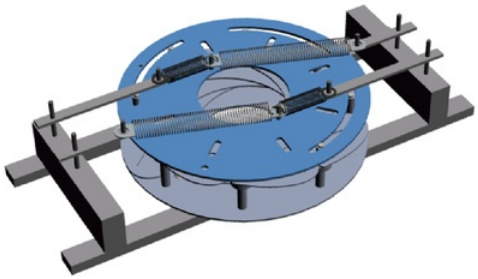

Figure 2.20: Experimental set-up for SMA spring aperture mechanism [30]

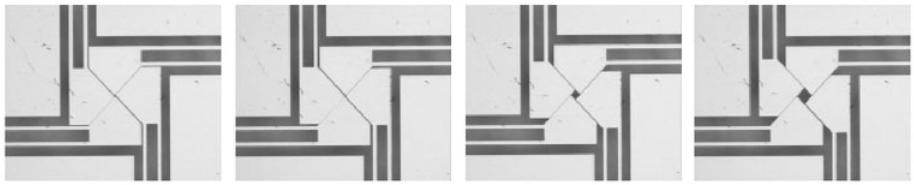

Figure 2.21: Sliding-blade MEMS variable aperture mechanism [34]

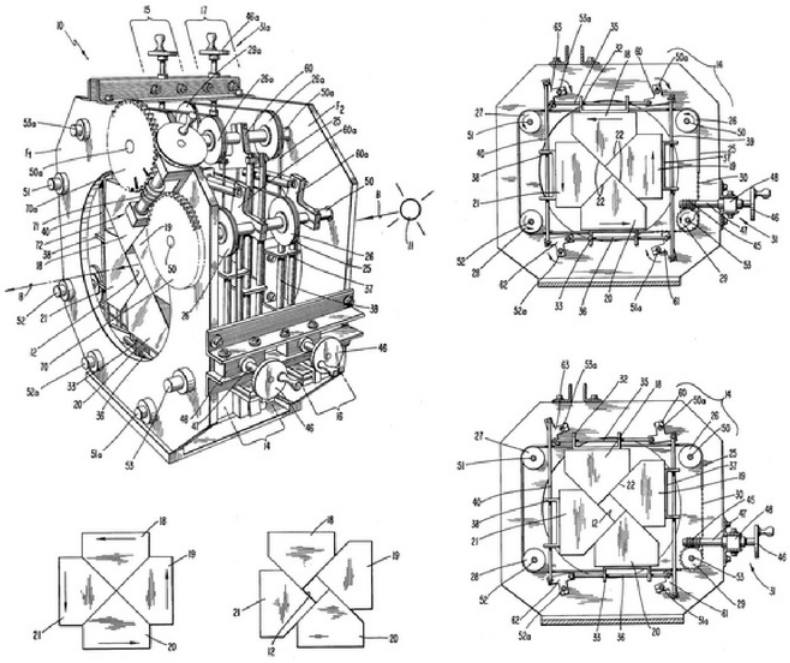

Figure 2.22: Variable aperture mechanism with 4 blocks actuated by gears [33]

2.4 Summary

A comprehensive overview of relevant technology and how it works has been provided. Specifically, this includes central receivers and their components, how heat is concentrated and distributed, as well as the effects of diffraction and aperture geometry. This information has been used to form the basis of key design decisions leading up to the creation of the aperture control mechanism detailed in this thesis. Previous work involving variable aperture mechanisms for solar and other applications has been summarised, revealing the uniqueness of the design of the present work, as will become increasingly evident in the coming chapters.

Chapter 3

The Squircle

3.1 Introduction

The stand-out feature that makes the mechanism described in this report unique is explained here. The use of the squircle shape as the profile for the variable aperture leads to a new way of approaching the problem of maintaining a circular opening. It allows for moving away from solutions involving approximation of a circle via polygons, in favour of continuous curves.

3.2 What is a squircle?

As the name implies, a squircle is an intermediate shape between a square and circle. It differs from a square with rounded corners in that there are no straight edges. Transitioning from a square to a circle, the corners become 4 mirrored parabolas. To clarify, the shape of each "corner" is governed by a varying parabolic equation, rather than a circular arc. These parabolas together form the squircle. See figure 3.2 for a visual representation of this transition between square and circle. A squircle's shape is governed by the equation:

$$x^2 + y^2 - \frac{s^2}{k^2}x^2y^2 = k^2 \tag{3.1}$$

where x and y are the coordinates along the horizontal and vertical axes on the Cartesian plane respectively, s is the squareness parameter and k is the radius or half length of the corresponding shape [35, 36]. For $s = 0$, the shape is a circle of radius k. For $s = 1$, the shape becomes a square of length $2k$. Any value of s between 0 and 1 yields a squircle.

3.3 Why is it relevant?

While attempts have been made to have an increasingly circular aperture for reasons mentioned in section 2.3.2 and 2.3.3 by adding more blades to an iris mechanism, there

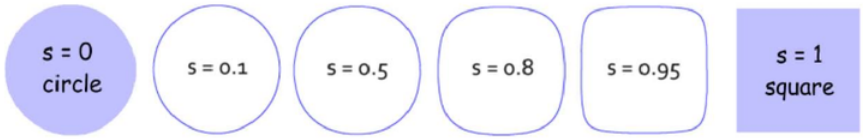

Figure 3.1: Transition between a square and circle by varying s [37]

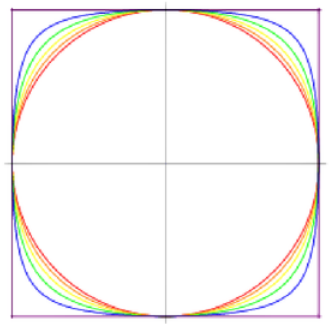

Figure 3.2: Superimposed squircle profiles [38]

is little in the literature about considering another shape entirely. In order to come up with a unique solution, the idea of trying to improve the multi-blade camera-like aperture was abandoned. Instead, research was conducted to find a shape that would behave like a circle in terms of the behaviour of light as it passes through the aperture.

Reiterating from section 2.3.2, a circular aperture is desired as it allows more radiation into the receiver than other shapes of the same area due to optical and heat transfer factors [12, 24]. In photography, if an aperture is non-circular and has edges, diffraction "spikes" of light radiating outwards from the centre of the image and overall blurring will result [27]. This just means that the light is being spread out. In the case of a solar receiver, this would cause some of the available light and thus heat, to not be captured.

Where the squircle comes in, is that it has been documented that moving from a square to a circle ($s = 1$ to $s = 0$), there is a point at which the diffraction pattern through an aperture becomes insensitive to changes in s [36]. Through both numerical [36] and experimental [39] means, this occurs somewhere between $s = 0.8$ and $s = 0.6$. It has been shown that small departures from a circular shape have little effect on diffraction through an aperture and that a squircle can mimic the properties of a circle very closely [36, 39]. See figure 3.3 for a numerical comparison between the diffraction patterns of squircles of $s = 0.8$ and 0.6, and a circle. In figure 3.4, an experimental comparison is shown.

Additionally, as described in section 2.3.2, a circle is ideal in terms of overlapping with regions of higher heat concentration as compared to other shapes due to the heat

distribution of the concentrated light being roughly circular. As is shown in figure 3.5, whilst a squircle may lose some regions of higher concentration as compared to a circle, it is still a better alternative to a square and can approximate a circle very closely depending on s.

In the aperture control mechanism of this thesis, the aperture is formed by 4 translating components that each have one quarter of a squircle as their leading profile. Therefore, instead of getting sharp edges as the aperture closes, with a squircle profile, what results is a squircle of varying radius and s across the transition from open to closed. Additionally, for most of the cycle, the s value is satisfactory for the application as defined above. See Chapter 4 for further details and Chapter 5 for a demonstration of this transition.

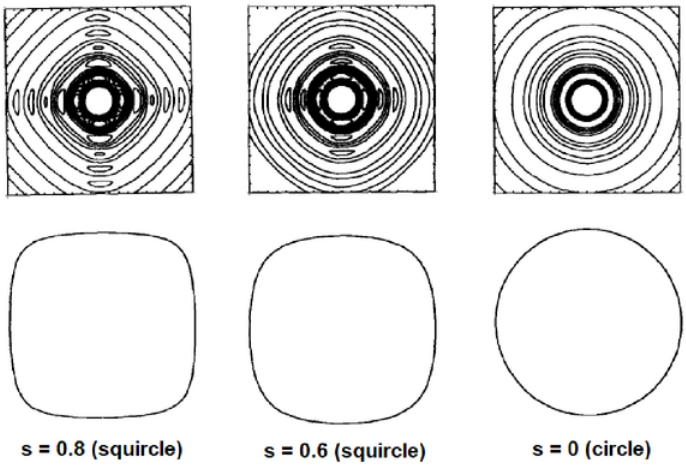

Figure 3.3: Diffraction patterns of squircles and circle [36]

In summary, though the squircle has been studied in relation to its similarities to a circle in terms of diffraction, nothing has been found in the literature linking the squircle to a variable aperture mechanism or solar technology. Therefore this thesis project is utilising a new concept entirely for controlling temperature in a solar receiver.

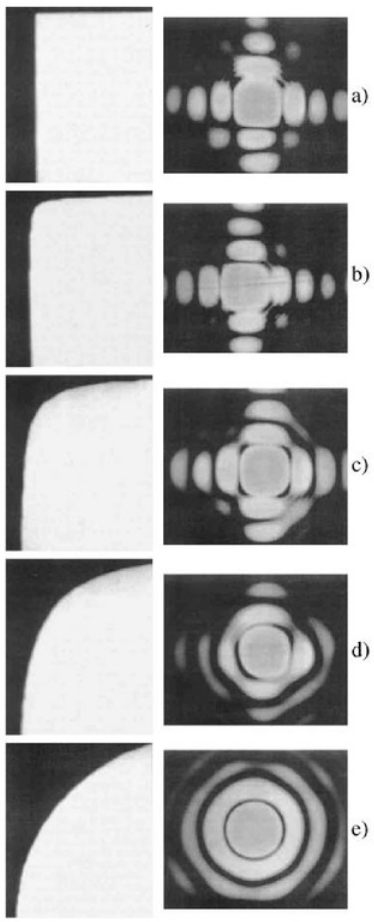

Figure 3.4: Experimental diffraction patterns of squircles: a) $s = 1.0$, b) $s = 0.995$, c) $s = 0.9$, d) $s = 0.8$, e) $s = 0.001$ [39]

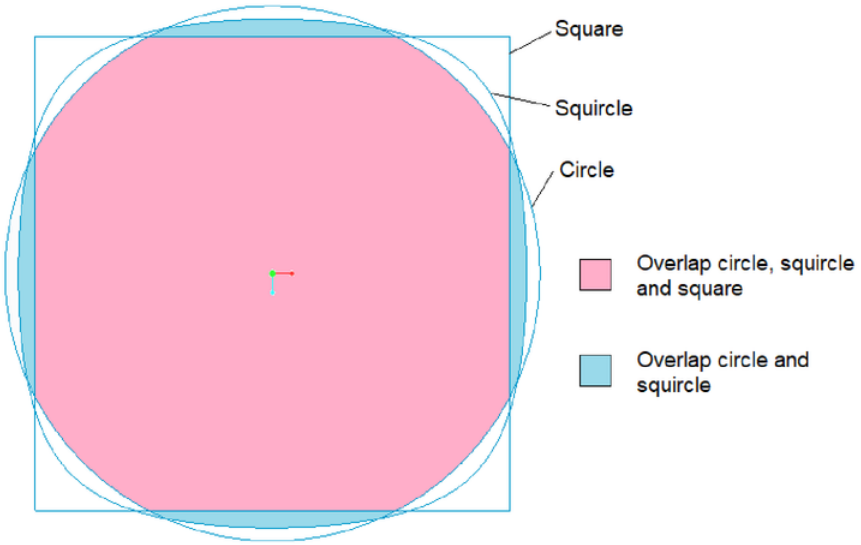

Figure 3.5: Comparing overlapping regions of a square, squircle ($s = 0.8$) and circle of same area

Chapter 4

The Mechanism

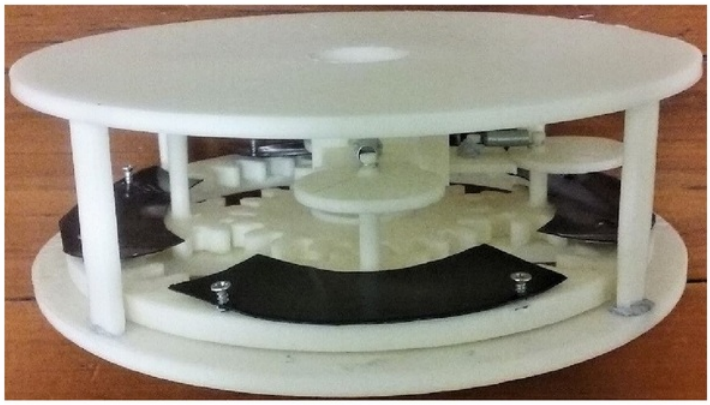

Figure 4.1: Fully assembled mechanism

In order to take advantage of the squircle for the aperture geometry as discussed in Chapter 3, a mechanism needed to be designed to achieve the necessary motion. This chapter provides a summary of the design process involved in the development of the final aperture control mechanism.

4.1 Design Features

4.1.1 Cams and Followers

Using a varying squircle for the aperture, a method of forming the shape was required. 4 components (followers), each with one quarter of an $s = 0.8$ squircle profile (see Chapter 3), were used. They are translated in 4 different directions, along 2 axes (see figure 4.4). These parts are called followers as their motion is governed by the rotation of cams. Figure 4.3 demonstrates how a cam changes the position of a follower as it rotates, with

a guide being used to keep the motion along one axis. A spring is used to return the follower to its original position when the cam has withdrawn.

As can be seen in the sketch of the cam used in the present work (fig. 4.2), since the axis of rotation (red dot) is not in the centre of the circle, as the cam is rotated, the follower is translated along its axis by a varying amount. In this case, the maximum displacement of the follower is 20mm.

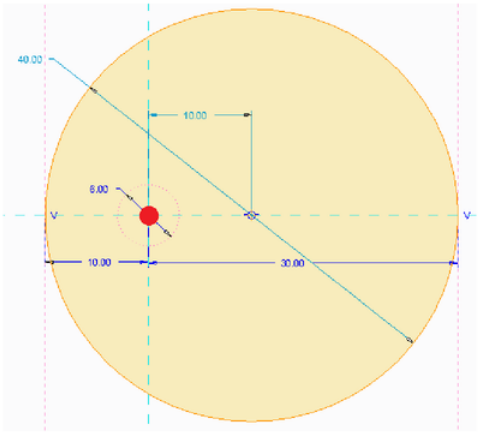

Figure 4.2: Cam sketch from present work

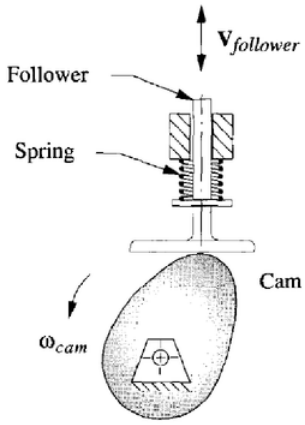

Figure 4.3: Diagram of cam, follower and spring assembly [40]

The solution in this report involves each cam being fixed to the top face of a planet gear via a support rod in a planetary gear assembly. See figure 4.6 for a basic schematic

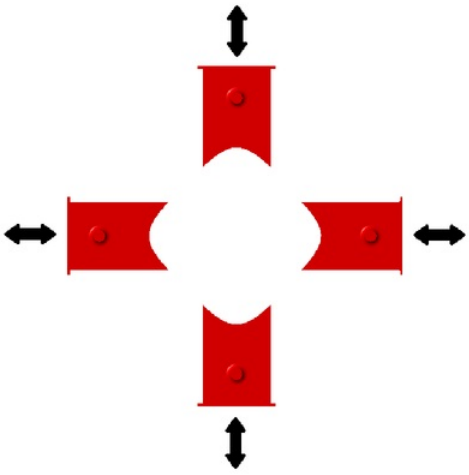

Figure 4.4: The directions of travel for the 4 followers

of a planetary gear set and the names for the different gears contained. The cams have the same rotation as the planet gears so when the ring gear is rotated, the sun and planet gears are also rotated, along with the cams. This controls the motion of the followers as they are pushed by cams and brought back by springs between the cams and followers. The springs are mounted to pivots, one on each cam and follower. See figure 4.5 for how the springs were mounted to the cams and followers in the present work.

Figure 4.5: Springs to return followers to resting position when cams move away

The previous concepts explored in the development of this mechanism utilised roller bearings instead of a planetary gear system to control the motion of the followers. This was abandoned due to the difficulty in achieving precise control over the rotation of the bearings and thus the cam-follower relationship, especially taking into consideration material and manufacturing constraints (see Chapter 6). Gears have teeth which mesh to ensure that dependent components rotate rather than slip as can be experienced with bearings.

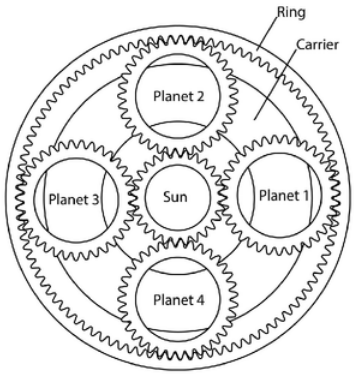

Figure 4.6: Schematic of planetary gear with four planets [41]

4.1.2 Planetary Gears

As stated previously, the rotation of the cams is governed by the planet gears in a planetary gear system. Thus, this system needed to be designed with the motion of the followers and the resulting aperture in mind.

Before performing any calculations for the gears, design constraints were considered. Firstly, a circle of 30mm diameter was chosen as the fully open aperture shape. Therefore a 30mm diameter hole would need to be going through the centre of the sun gear. This meant that the sun gear had to be wide enough to maintain rigidity and strength despite having the hole. It was decided that the pitch diameter would be 80mm to also account for grooves cut in for meshing teeth of other gears.

The module (m) of a gear is defined as the ratio of its pitch diameter (D_p) to number of teeth (N). Therefore, $m = \frac{D_p}{N}$ and $N = \frac{D_p}{m}$. Since the prototype was to be 3D printed in plastic, with limitations in terms of strength and accuracy, fewer and larger teeth was the favoured option. With higher m, N is reduced for the same D_P. $m = 4$ was chosen as the module, which is identical for all gears so that they mesh properly.

Next, it was decided that D_p of the planet gears would be 40mm. They would need to have enough room on the top face to attach to cams but also not be so big that the mechanism was too large overall. From this, the ring gear was fixed at $D_p = 160$mm since it circles 2 planets and the sun across each axis: $80 + 2 \times 40 = 160$.

From there, the rest of the gear properties were calculated based on equations in tables 4.1 and 4.2 [42, 43]. See figure 4.7 for a diagram of some of the terms used to define spur gears. It is similar for ring gears, except that the addendum and dedendum are reversed (see figure 4.8).

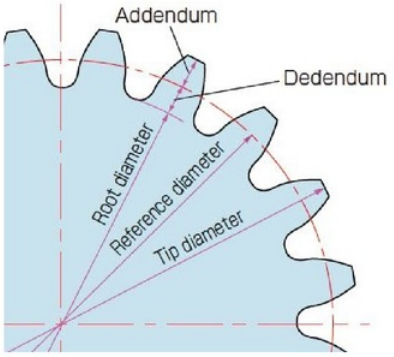

Figure 4.7: Nomenclature for spur gears [43]

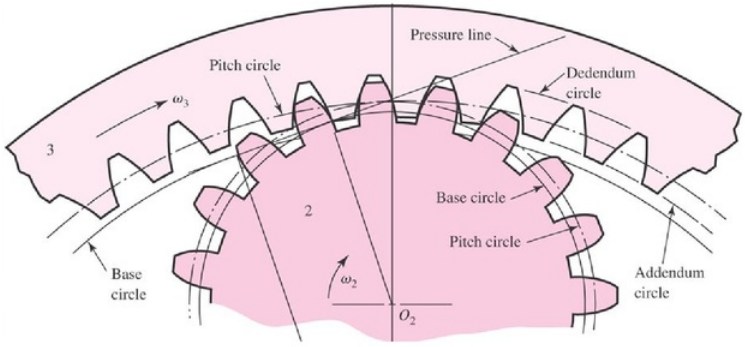

Figure 4.8: Nomenclature for ring gears [44]

The next thing to calculate was the gear ratio between the planets and ring of the designed system. Let n be the number of revolutions and N be the number of teeth, with r, s and p being the subscripts for the ring, sun and planet gears, respectively. The equation [45] is therefore:

$$n_p = \frac{N_r}{N_p} n_r \tag{4.1}$$

Taking n_r as 1 revolution, and having already calculated $N_r = 40\text{mm}$ and $N_r = 10\text{mm}$, $n_p = \frac{40}{10}(1) = 4$. Therefore, for every 1 revolution of the ring gear, each planet gear rotates 4 times. This allows for controlling the motion of the cams and followers to vary the aperture using ring gear rotation.

Table 4.1: Spur gear calculations

Item	Symbol	Formula	Sun	Planet
Module (mm)	m	Chosen	4	
Pressure Angle (deg)	α		20	
Pitch Diameter (mm)	D_p		80	40
Addendum (mm)	a	1.00m	4	
Dedendum (mm)	b	1.25m	5	
Tooth Depth (mm)	h	2.25m	9	
Number of Teeth	N	$\frac{D_p}{m}$	20	10
Tip Diameter (mm)	D_t	D_p+2m	88	48
Base Diameter (mm)	D_b	$D_p\cos\alpha$	75.18	37.59
Root Diameter (mm)	D_r	D_p-2.5m	70	30

Table 4.2: Ring gear calculations

Item	Symbol	Formula	Ring
Module (mm)	m	Chosen	4
Pressure Angle (deg)	α		20
Number of Teeth	N		40
Addendum (mm)	a	1.00m	4
Dedendum (mm)	b	1.25m	5
Tooth Depth (mm)	h	2.25m	9
Pitch Diameter (mm)	D_p	Nm	160
Tip Diameter (mm)	D_t	D_p-2m	152
Base Diameter (mm)	D_b	$D_p\cos\alpha$	150.35
Root Diameter (mm)	D_r	D_p+2h	170

The carrier holds the planet gears and can also be used to hold the rest of the gears. In the case of this mechanism, the carrier does not rotate independently of the ring and sun gears. Therefore it is considered "fixed". In planetary gear systems, there are always two inputs and one output. In this case, the planets are the output since the carrier is fixed. Therefore the ring and sun gears are the inputs.

4.2 CAD Modelling

CAD models of the designed parts are presented here in order to illustrate the design process as well as clarify how the components interact to make the mechanism function. The final design (Design 3) is featured, but earlier Designs 1 and 2 are briefly shown to demonstrate the design progression through iteration.

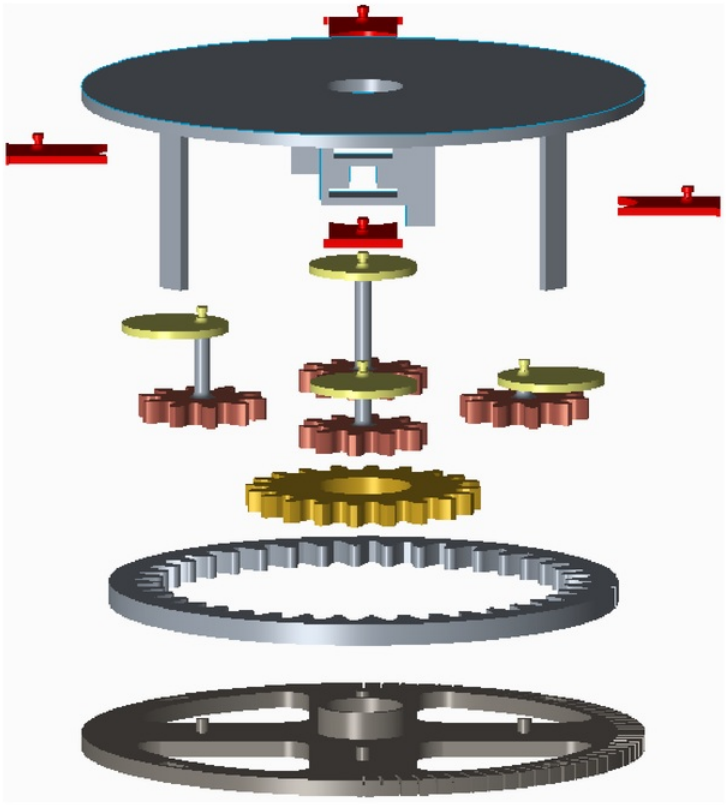

Figure 4.9: Exploded view of Design 3 with all components disassembled

4.2.1 Gears and Followers

Since the gears and followers are the most important components of the mechanism, a brief description of how they were modelled is provided here.

Gears:
Based on the calculations from table 4.1 and a drawing guide [46], the sun gear was

drawn. Firstly, the circles (pitch, tip, base and root) were sketched (figure 4.11a). Then the involute curve was drawn. This is a mathematical shape used to form the gear tooth profile. The curve goes outwards from the base circle and is defined by the equations in figure 4.10. The only user-defined parameter is r which is the radius of the base circle ($D_b/2$). The rest are dependent variables.

```
x = t
ang = t * 90
s = (3.1416 * r * t) / 2
x = r * cos(ang) + (s * sin(ang))
z = r * sin(ang) - (s * cos(ang))
y = 0
```

Figure 4.10: Involute curve equations

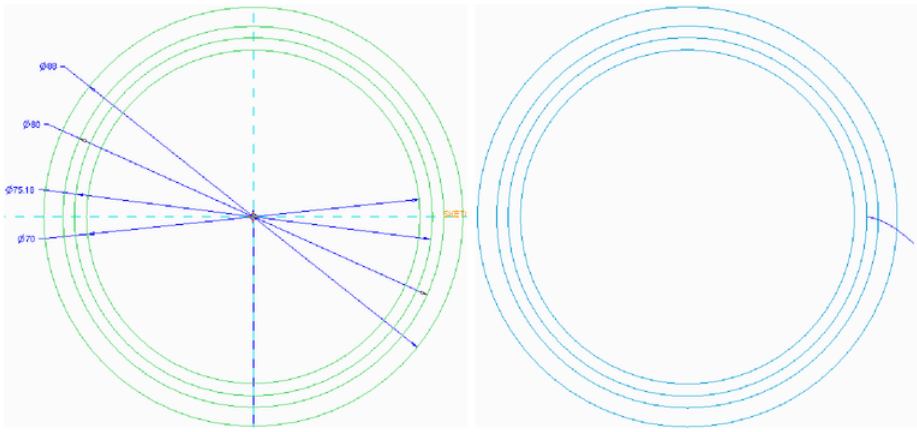

(a) Pitch, tip, base and root circles **(b)** Involute curve for gear teeth

Figure 4.11: Drawing the sun gear circles (a), and involute curve (b)

The involute curve was then mirrored 18° away (dividing 360° by $N = 20$ teeth). Trimming the curves at the tip circle forms the outside of the tooth. This was copied evenly around the circle 20 times to create the correct number of teeth (see figure 4.12). The next steps involved removing material to allow for meshing with teeth from connected gears (planets). See figures 4.13 and 4.14. Lastly, a circle of diameter 30mm was cut out of the middle so as not to block the aperture created by the follower (figure 4.15).

A similar process was followed for the planet and ring gears, except that with the ring gear the teeth were cut from a solid circle rather than extruded out from it. The teeth are internal.

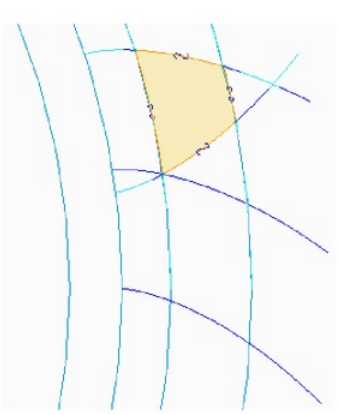

(a) Tooth profile sketch

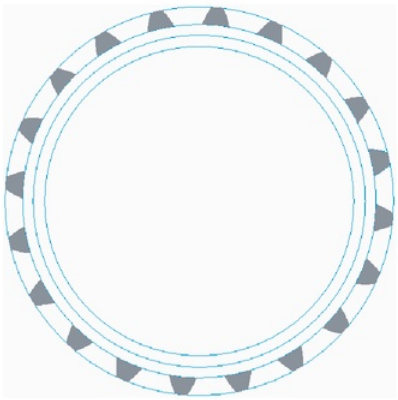

(b) Tooth pattern based on number of teeth ($N = 20$)

Figure 4.12: Drawing the gear teeth

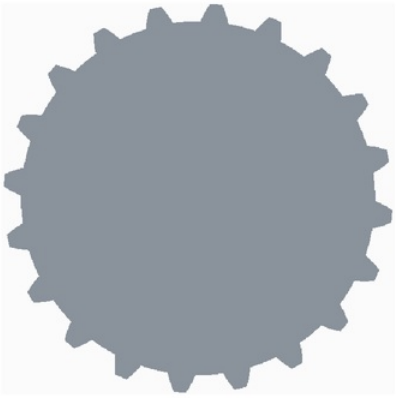

(a) Solid gear with external teeth

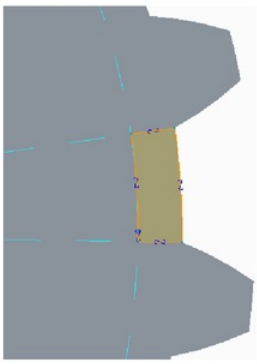

(b) Sketch to remove material for full tooth profile

Figure 4.13: Finishing gear teeth

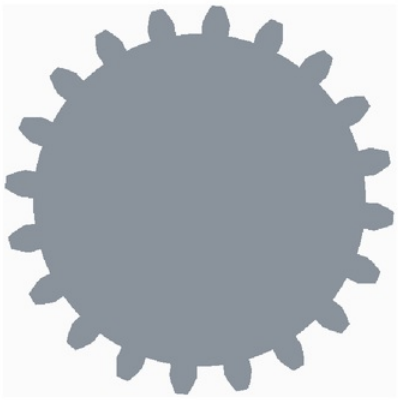

(a) Gear with finished tooth pattern

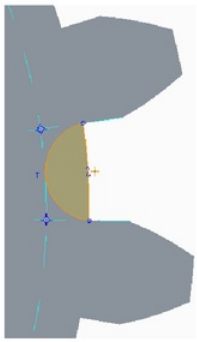

(b) Sketch to remove material for gear meshing

Figure 4.14: Finishing the gear geometry

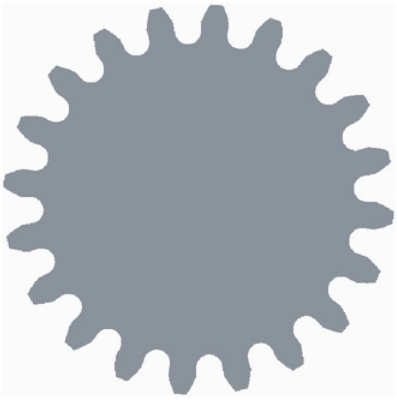

(a) Fully functional gear

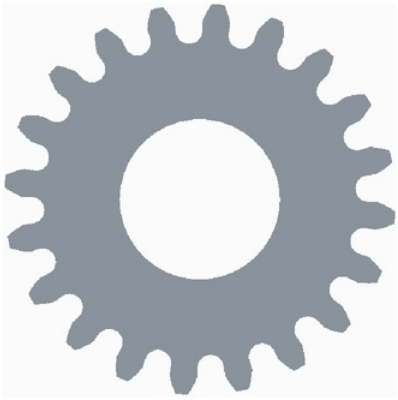

(b) Circle cut out for aperture

Figure 4.15: Completed sun gear

Followers:
The key feature of each follower is the quarter of a squircle profile that forms the aperture as a whole as the four followers come together. In creating the follower component, this squircle curve was drawn first. The squircle equation 3.1 was converted into a form that Creo Parametric could understand and s and k values set (see figures 4.16 and 4.17).

```
x=t
z=sqrt((r^2-t^2)/(1-s^2/r^2*t^2))
```

Figure 4.16: Squircle equation in modelling form

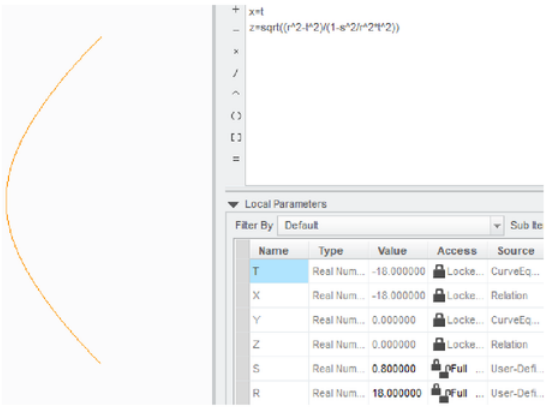

Figure 4.17: Drawing the squircle curve: $s = 0.8$, $k = 18$mm (k shown as r)

The squircle curve was then connected to a full sketch of the part so that a solid could be formed. Lastly, features such as the spring pivot and a flange to keep the followers in the guides were drawn. See figure 4.18.

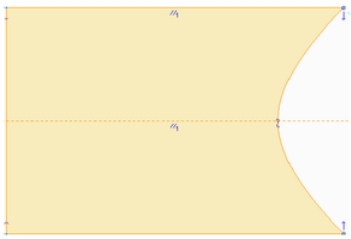

(a) Top sketch with squircle curve

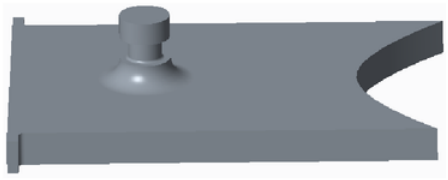

(b) Completed part with spring pivot and flange

Figure 4.18: Follower

4.2.2 Assembly

This section presents the components and demonstrates how they work together.

Three designs were created in order to reach the final outcome (Design 3). All were based on rotating cams to translate followers, but the previous designs relied on roller bearings to rotate the cams. Design 3 uses a planetary gear system, so instead of having an "inner ring" with rollers, a "carrier" is used to hold the gears. The top cover with follower guides fits into the grooves cut into the top face of the carrier. See figures 4.19 and 4.21.

Other features of the carrier include the hole in the middle for light to pass through, 4 cut-outs to save material and notches that line up with a notch on the ring gear to keep track of gear rotation and thus follower motion (see figure 4.20). These notches are important as each one is 3.75° apart on the carrier. Since the ratio of rotation of ring gear to planet gear (and thus cam) is 1:4, by moving the ring gear one notch, the cam is rotated by 15°. The notches were used to have discrete positions in which to test the aperture control mechanism. See Chapter 5 for more detail.

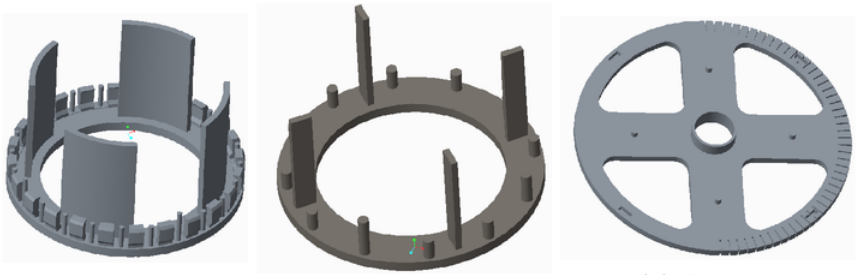

(a) Design 1 **(b)** Design 2 **(c)** Design 3

Figure 4.19: Inner rings of Designs 1 and 2 and carrier of Design 3

A planetary gears system consists of sun, ring and planet gears. Since the mechanism involves 4 pairs of cams and followers, 4 planet gears were used (see figure 4.22). The sun gear in this case has a circle cut in the centre to allow light to pass through, only restricted by the translating followers as explained earlier.

Each cam was joined to the top face of a planet gear via a rod. This way, the part was 3D printed as one piece. The cam pushes on the follower which is restricted to one-axis motion by guides on the top cover. An extension spring hooks onto the spring pivots of the cam and follower to keep them constantly in contact. See figure 4.23 for the arrangement of planet gear, cam and follower and figures 4.24 and 4.25 for the mechanism cover with follower guides. The top cover also has a hole so as not to obstruct incoming light.

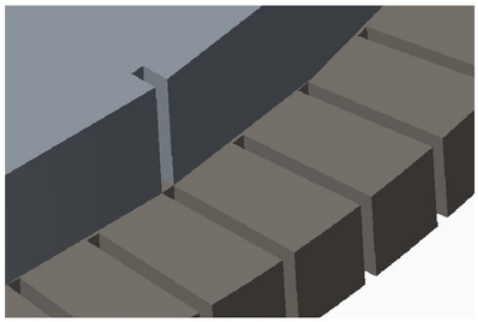

Figure 4.20: Ring gear notch lines up with notches on carrier

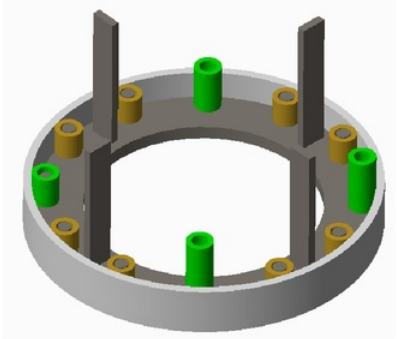

(a) 2: Inner ring, outer ring and rollers assembled

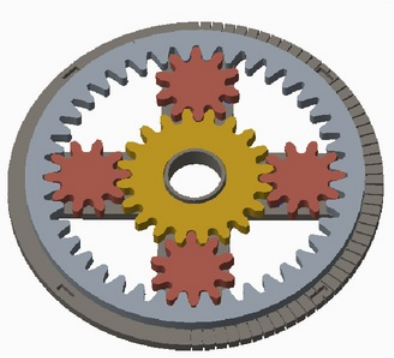

(b) 3: Carrier with gears

Figure 4.21: Designs 2 (a) and 3 (b) base assemblies

For visualisation of the mechanism at work, see figure 4.26 which shows how different positions of the cam lead to different positions of the followers, therefore controlling the aperture. The cover is hidden for clarity. Figure 4.27 is the fully assembled Design 3 CAD model (see figure 4.9 for an exploded view) and figure 4.28 shows the previous designs.

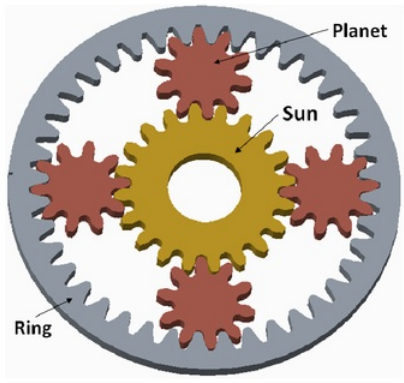

Figure 4.22: Labelled arrangement of gears

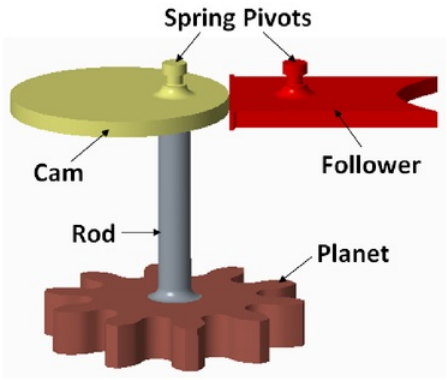

(a) Cam-follower and planet gear assembly

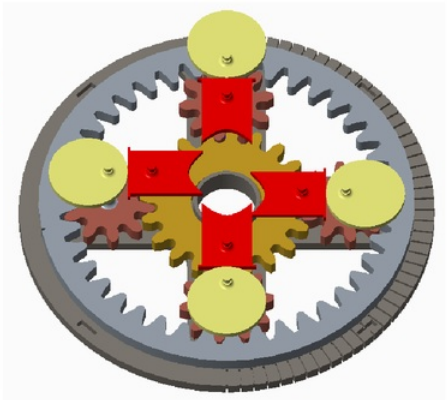

(b) Fully assembled without the top cover with guides

Figure 4.23: Relationship between gears, cams and followers on carrier base

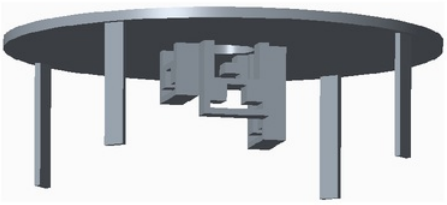

(a) Cover

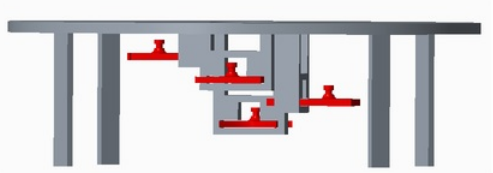

(b) Cover with followers in guides

Figure 4.24: Cover with legs for fitting into carrier and guides for followers

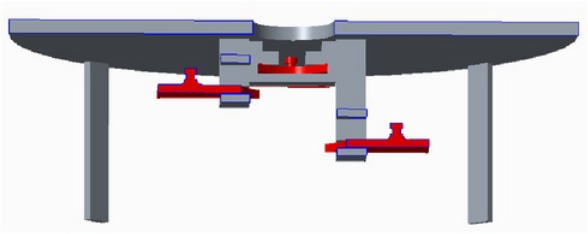

Figure 4.25: Section view of top cover with guides for followers

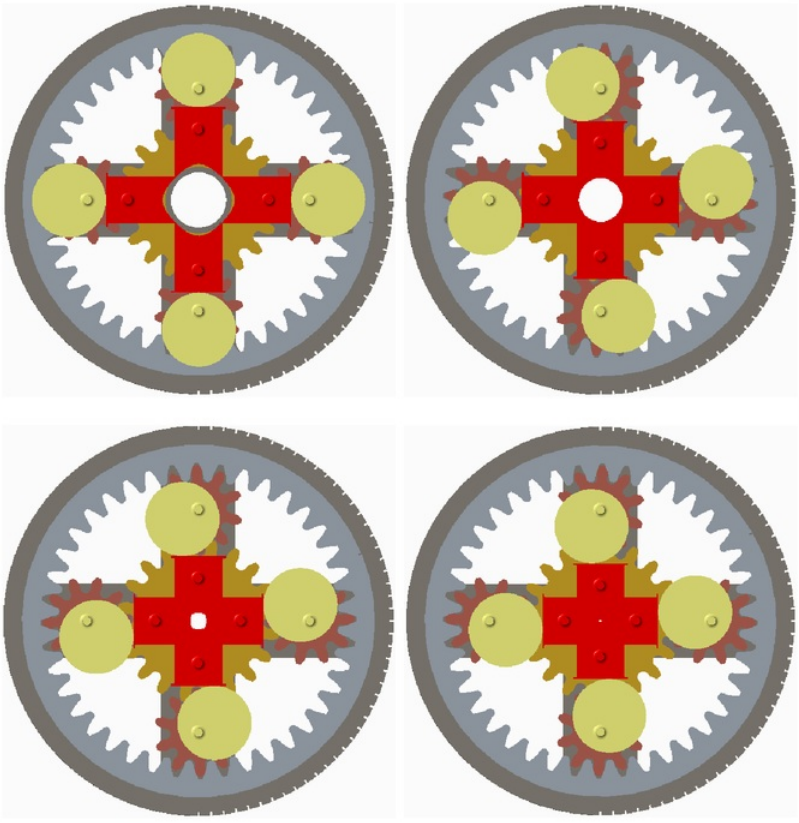

Figure 4.26: Mechanism with cover off in different positions

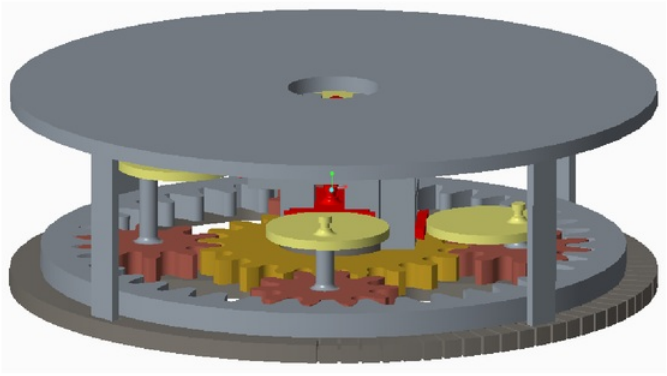

Figure 4.27: Complete CAD model of Design 3

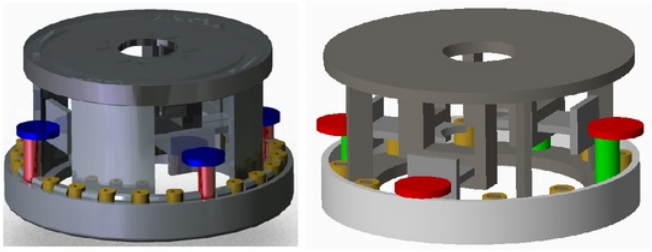

(a) Design 1 **(b)** Design 2

Figure 4.28: Fully assembled CAD models of Designs 1 and 2

4.3 Summary

A complete aperture control mechanism involving cams, followers and planetary gears was developed from basic design assumptions, leading to calculations and then a full 3D model. The component models were drawn dimensionally accurate, allowing them to be utilised in both the analytical and experimental stages of verifying its efficacy (see Chapters 5 and 6).

Chapter 5

Analytical Methodology

In order to verify that temperature control could be achieved through the use of the designed mechanism, quantitative analysis of the motion of components was required. This chapter details the properties of the aperture as the mechanism transitions it from open to closed. This includes the position of the cams and followers, the area of the aperture and the squareness s of the shape the overlapping followers form. From this data, comparisons can be made and relationships defined between temperature results and aperture properties which is crucial in judging the

5.1 Cam and Follower Motion

As explained in previous chapters, the position of the cam as it rotates directly affects the linear position of the corresponding follower. To quantify this relationship, specific notches on the carrier and ring gear (see figure 4.20) have been numbered based on the aperture properties at that position. Notch 0 is the notch where the ring gear notch lines up with a carrier notch such that the followers are at their furthest away from the centre of the mechanism, not yet overlapping the aperture area (see figure 5.3a). Though this is not relevant for testing as Notch 1 leads to the same aperture geometry, it is useful in analysing the changing s and area of the aperture through the follower motion.

In table 5.1, each notch is defined in relation to Notch 1, which is taken as being at the 0° position of the cam since it is the position at which the aperture area is maximum. Each subsequent notch is 15° (cam position) from the previous as explained in section 4.2.2. See figure 5.1 for the set of notches as defined in table 5.1. Whilst Notch 9 is the notch at which the aperture is fully closed according to the CAD model (see table 5.4), due to the closeness of Notch 8 to 0 area and inaccuracies in 3D printing and notch line-up, physically Notch 8 corresponded to 0 area of the prototype. Therefore, 105° of cam rotation was the full range used in testing, between Notch 1 and 8.

Each notch corresponds to a follower position. This position is defined as the pivot distance, the distance between the spring pivots of the cam and follower pairs (figure 5.2).

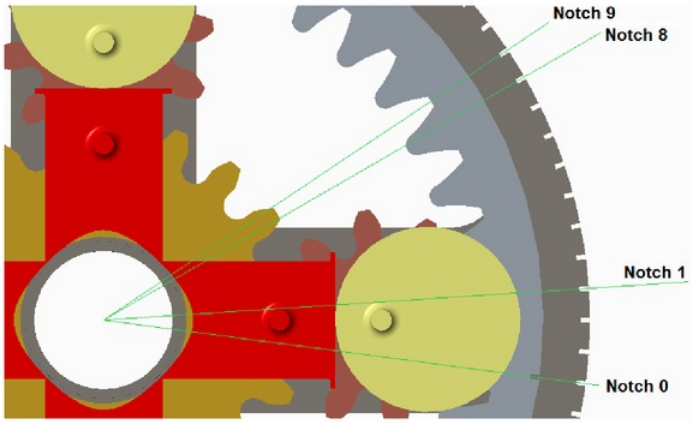

Figure 5.1: Pivot distance (black arrows) varies throughout mechanism motion but is identical for all cam-follower pairs

Table 5.1: Distance between pivots for each notch

Notch	Position (degrees)
0	-45
1	0
2	15
3	30
4	45
5	60
6	75
7	90
8	105
9	120

This was measured and is tabulated in table 5.2. The relationship between notch and pivot distance is roughly linear (see figure 5.4).

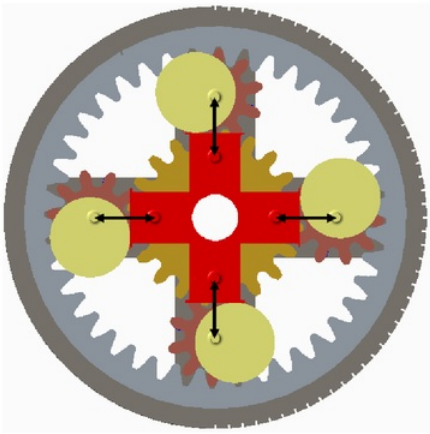

Figure 5.2: Pivot distance (black arrows) varies throughout mechanism motion but is identical for all cam-follower pairs

Table 5.2: Distance between pivots for each notch

Notch	Pivot Distance (mm)
0	22.00
1	25.03
2	27.13
3	29.55
4	32.15
5	34.74
6	37.13
7	39.18
8	40.74
9	41.70

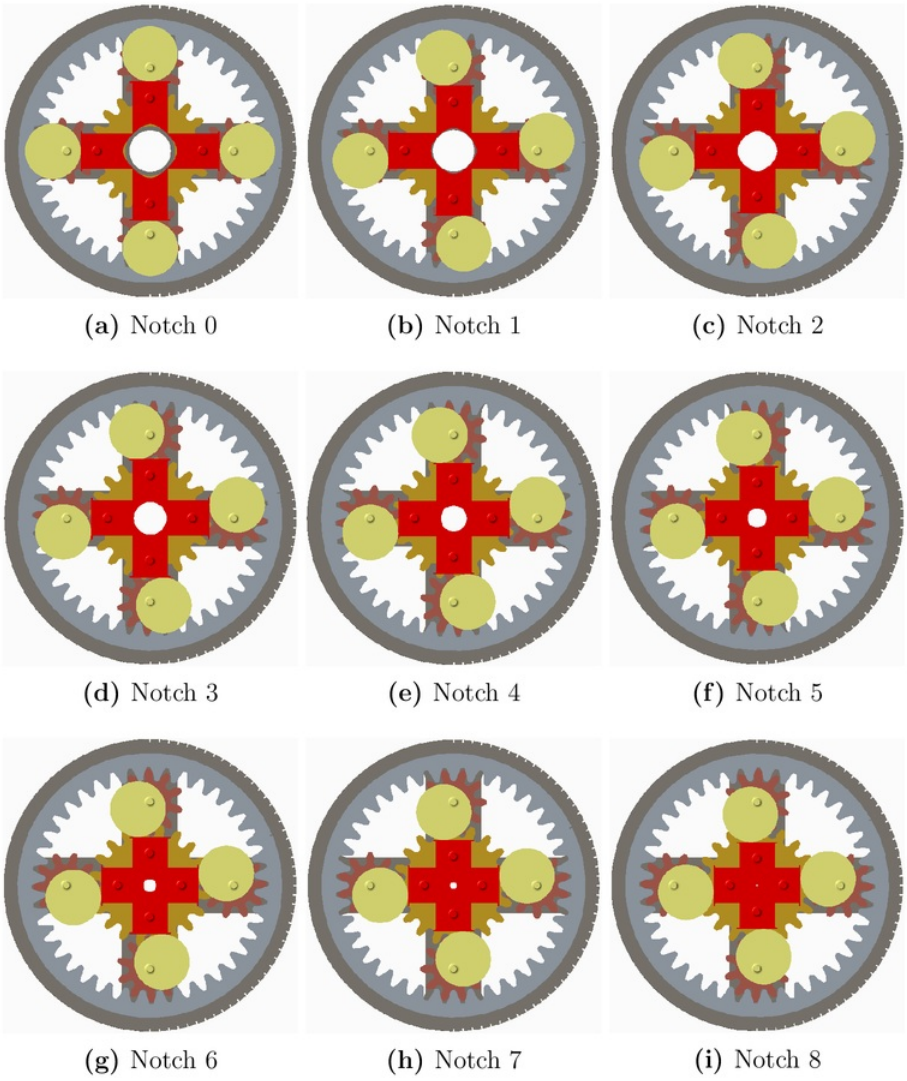

(a) Notch 0 **(b)** Notch 1 **(c)** Notch 2

(d) Notch 3 **(e)** Notch 4 **(f)** Notch 5

(g) Notch 6 **(h)** Notch 7 **(i)** Notch 8

Figure 5.3: Mechanism with the cover off transitioning between fully open and fully closed in the defined notch positions

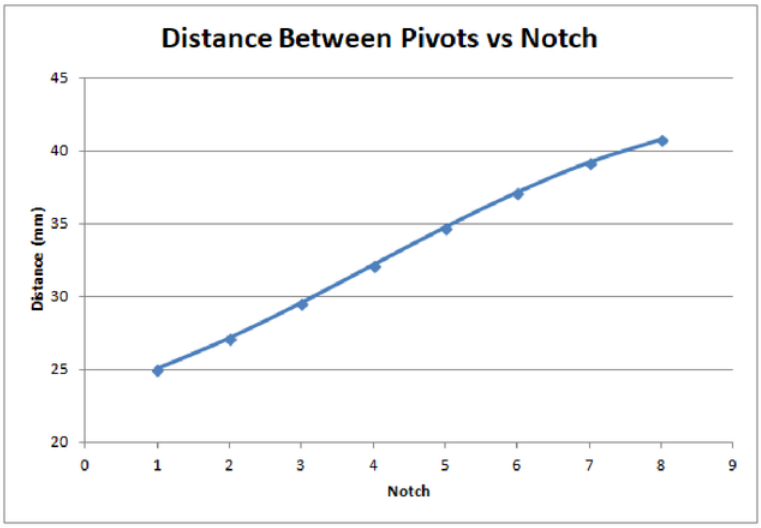

Figure 5.4: Graph of distance between cam and follower spring pivots for all notches

5.2 Area and Squareness

As defined in Chapter 3, a squircle is a shape between a square and circle. In order to calculate s (squareness parameter) and area of the aperture for each notch position, there must be an approximate squircle defined for each position.

Rearranging equation 3.1 for a squircle, the equation to calculate s is:

$$s = \sqrt{\frac{k^2(x^2+y^2) - k^4}{x^2y^2}} \tag{5.1}$$

where k and x are as defined in figure 5.5. Since a squircle is symmetric about the x and y axes, taking the point at the "corner", $x = y$. Therefore, the equation becomes:

$$s = \sqrt{\frac{2k^2x^2 - k^4}{x^4}} \tag{5.2}$$

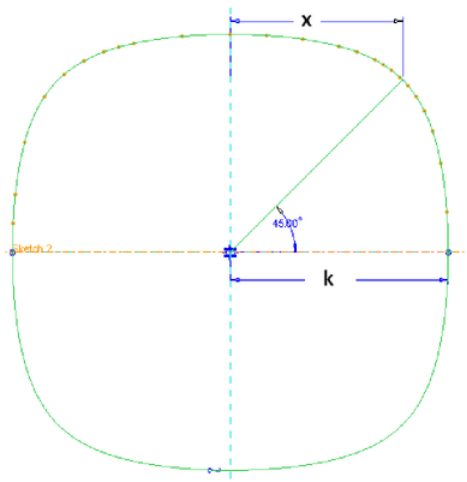

Figure 5.5: Squircle dimensions

To find k and x for each notch, the follower curve in the assembled CAD model was projected onto a sketch, where distances could be measured by drawing appropriate lines (see figure ??). The same was done for all notches and s was calculated, yielding the data in table 5.3.

The values for k and s from table 5.3 were used to draw an approximate squircle for the aperture at each notch. This followed the same process as outlined in section 4.2 for the follower profile. See figures 5.7 and 5.8 for the results of this. These closed shapes

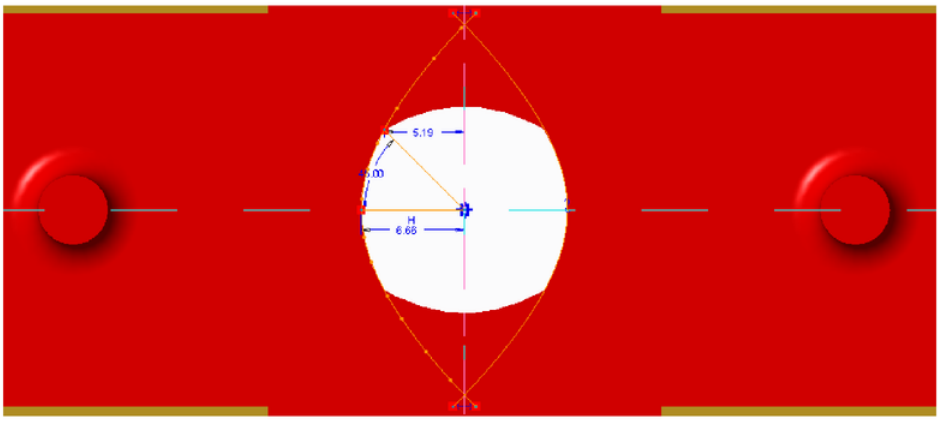

Figure 5.6: Measuring k and x for notch 5 ($k = 6.66$ and $x = 5.19$)

Table 5.3: s, k and x values for each notch

Notch	k (mm)	x (mm)	s
0	17.48	13.71	0.78
1	15.00	10.61	0.00
2	13.68	10.08	0.54
3	11.83	8.32	0.21
4	9.24	6.80	0.53
5	6.66	5.19	0.76
6	4.26	3.55	0.90
7	2.22	1.99	0.97
8	0.66	0.64	1.00

were then used to measure the aperture area using an in-built tool in Creo Parametric. See table 5.4. Figures 5.10 and 5.9 put the relationships between notch and s and notch and area in graphical form.

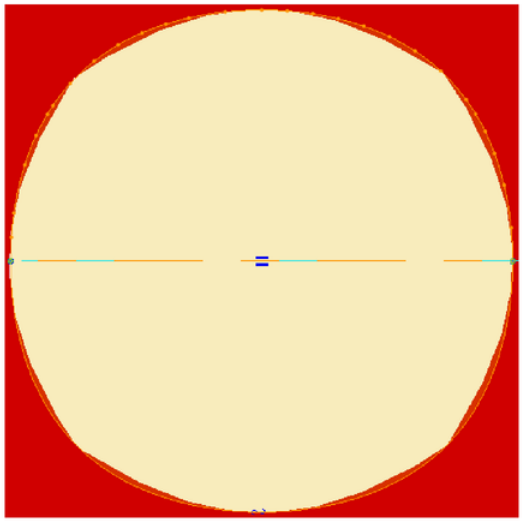

Figure 5.7: Notch 4 approximate shape zoomed in. The orange outline is the sketch and the red sections are where the followers overlap

Table 5.4: Approximate aperture area for each notch

Notch	Area (mm^2)
0	1058.21
1	706.86
2	612.05
3	442.05
4	278.74
5	152.63
6	66.17
7	18.90
8	1.75
9	0.00

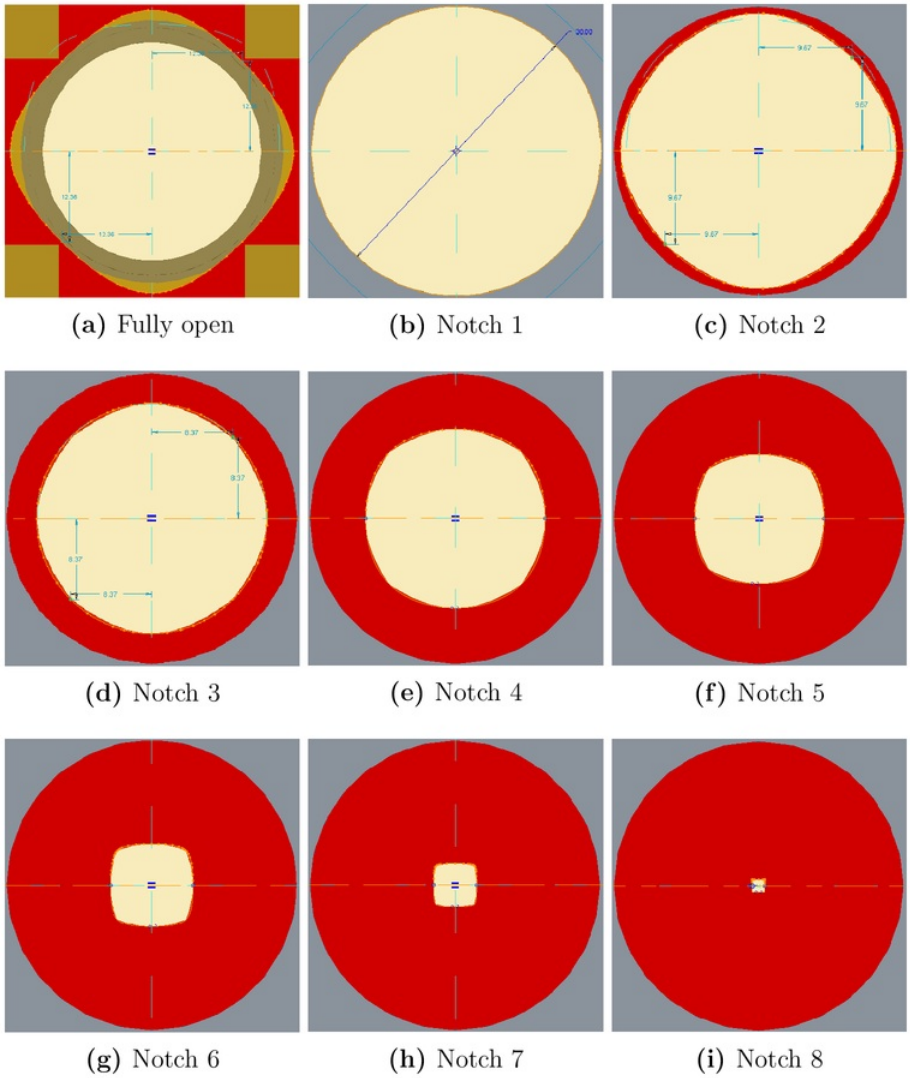

(a) Fully open (b) Notch 1 (c) Notch 2

(d) Notch 3 (e) Notch 4 (f) Notch 5

(g) Notch 6 (h) Notch 7 (i) Notch 8

Figure 5.8: Approximate squircle shapes for the aperture at each notch

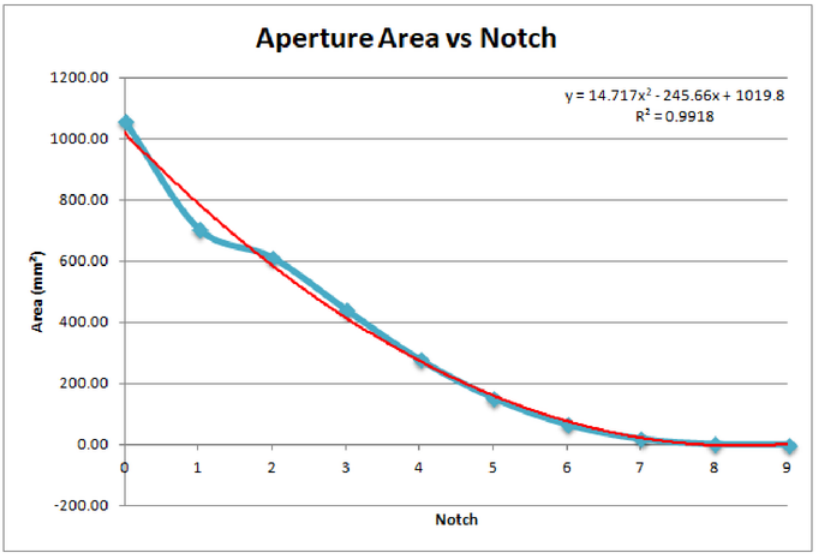

Figure 5.9: Graph of aperture area for each notch

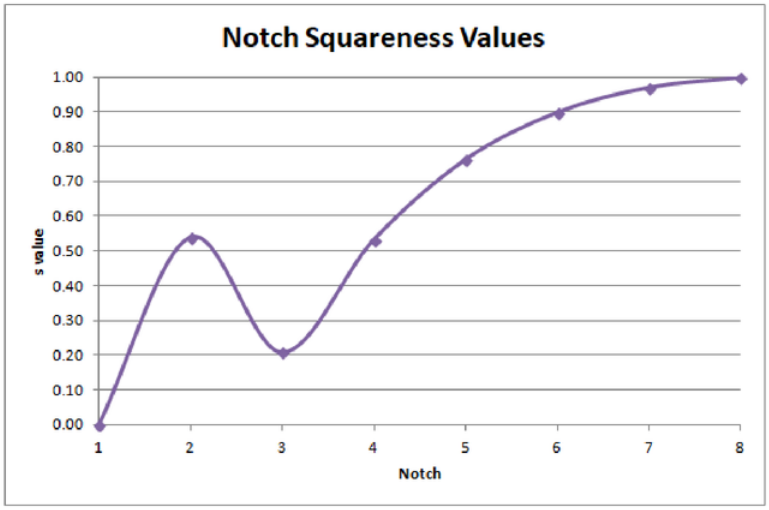

Figure 5.10: Graph of aperture squareness for each notch position

Chapter 6

Experimental Methodology

6.1 Prototyping

A prototype based on the CAD models shown in section 4.2 was created using the OMNI3D Factory 2.0 Production System. CAD files were converted to stereolithography (.stl) files for 3D printing. Imported models were arranged on the system's print layout digital display, giving a preview of how parts would be printed (fig. 6.2). Settings such as part density (25%), support material density (25%) and number of top and bottom solid layers (5) were entered before commencing.

Parts were printed using acrylonitrile butadiene styrene (ABS) plastic. Support material was printed with the actual part geometry in order to support the structure as it is formed layer by layer (fig. 6.3). Once printing was completed, parts were cleaned of support material so that they could be properly assembled. Black pieces of plastic were cut to fit over the ring gear and screwed into it, acting as "guards" to prevent planet gears from popping up when pulled on by springs during aperture closing (see fig. 6.4). Finally, assembly of gears and the attachment of springs between the cams and followers on the pivot points was completed, forming the final prototype (see fig. 6.5).

Prototype 3 worked as designed. The previous prototypes 1 and 2 were based on a roller bearing system and were non-functional. Prototype 1 was not fully assembled due to printer errors causing the top cap part to fail and rollers not being able to fit on the rods of the inner ring. Prototype 2 was fully assembled but non-functional due to rollers sliding along the outer ring rather than rotating. This led to the decision to substitute roller bearings with planetary gears.

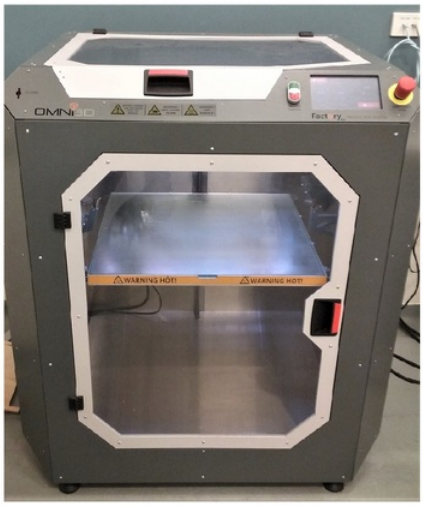

Figure 6.1: OMNI3D Factory 2.0 Production System

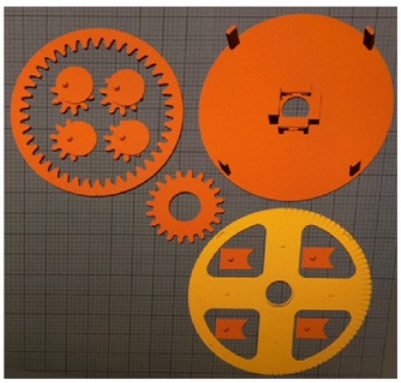

(a) Layout of parts to be printed

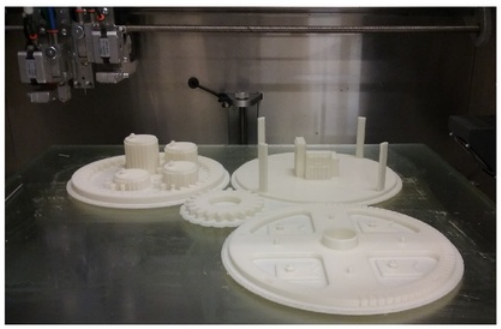

(b) Printed parts with support material

Figure 6.2: Files to printed parts

Figure 6.3: Parts with support material and cleaned part

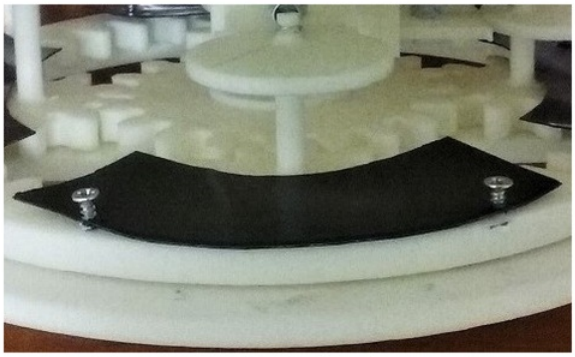

Figure 6.4: Plastic “guards” for planet gears (black)

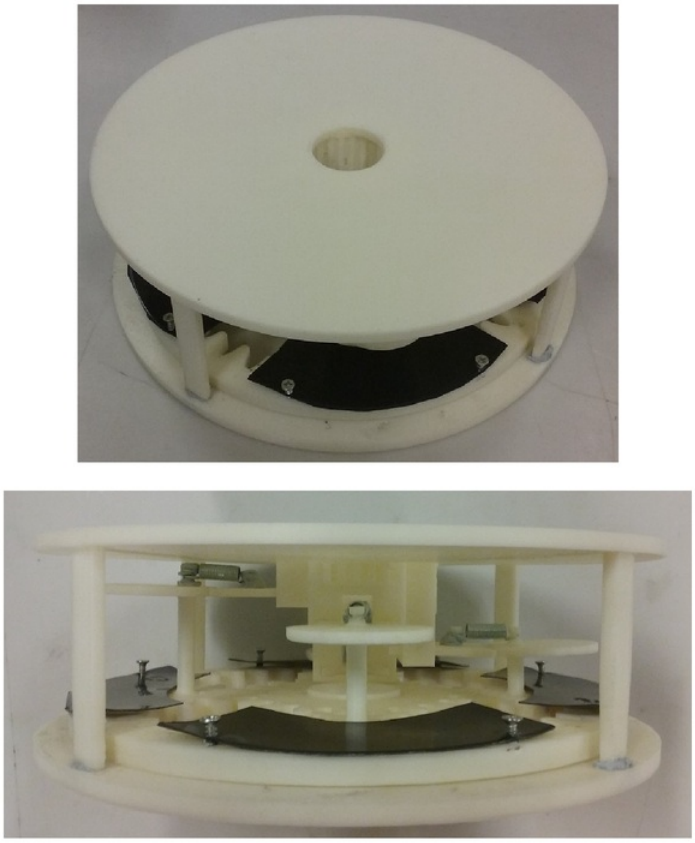

Figure 6.5: Prototype 3 completed

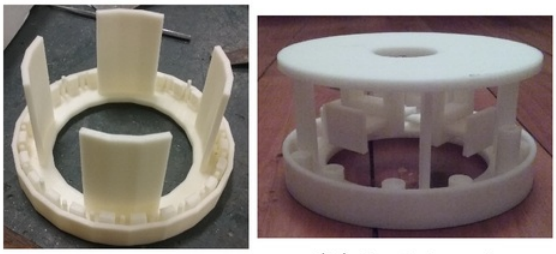

(a) Prototype 1 **(b)** Prototype 2

Figure 6.6: Previous prototypes

6.2 Experimental Set-up and Testing

The aperture control mechanism, once fully fabricated and assembled, was tested for its ability to control the temperature in a mock receiver. A solar simulator consisting of a 300W Xenon arc lamp Y1089 with power supply and electric current controller was used as the heat source (fig 6.7). The "receiver" was a closed plastic container, lined with tin foil and black tape to keep it well insulated. A hole was drilled in the middle of the cap for a thermocouple, secured and sealed in place using Bostik Blu Tack. See figure 6.8 for the assembly of receiver components and its position in testing.

An RS-1327K Infrared Thermometer with thermocouple attachment was used to measure the temperature inside the receiver. A digital readout was used to measure both a fixed point for room temperature (bottom reading) and the thermocouple sensor data (top reading). See figure 6.9. The mechanism was fixed in different positions using bulldog clips (fig. 6.10) according to notches as described in Chapter 5 so that temperature could be compared directly to aperture properties.

For the experimental set-up, the aperture control mechanism was placed above the receiver with thermocouple inside. The centre of the aperture was lined up with the centre of the receiver for incident light to reach the receiver. The solar simulator lamp was placed above the mechanism, resting on packaging material with a hole cut for the light to pass through. the centre of the light source was also lined up with aperture and receiver. See figure 6.11 for this set-up and figure 6.12 for how the light shines over the aperture.

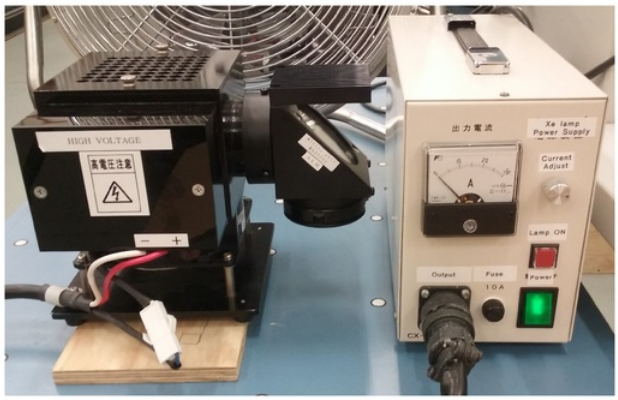

Figure 6.7: Solar simulator: lamp (left), power supply and current controller (right)

Three settings for current were used in testing; 10, 15 and 20 amperes (A). This was controlled using the current adjust dial for the solar simulator. Higher current corresponds to higher power density, and therefore heat. The relationship between current and power density for the Xenon lamp was determined in previous experimentation (see table 6.1). All notch positions were tested for 10A and 15A but 20A did not have the full set tested due to the temperature being too high for the materials (see Chapter 7).

Table 6.1: Power density of Xenon lamp for different currents

Current (A)	Power Density (mW/cm^2)
10	8.14
15	351.76
20	671.14

In all cases, testing was started with the components at room temperature, with this temperature recorded. Once the simulator was turned on, timing was started. For the first 10 minutes, the temperature was taken every 10 seconds, then every 30 seconds until 20 minutes, then once a minute for the remaining time. The tests were run for a total of 40, 45 and 50 minutes for the 10, 15 and 20A settings, respectively. This is because it was found that with higher heat, the temperature took longer to stabilise.

Figure 6.8: Mock receiver assembly

Figure 6.9: Thermometer and thermocouple attachment

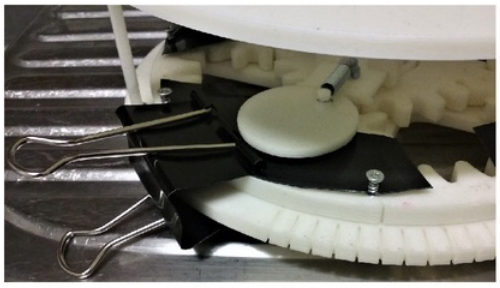

Figure 6.10: Mechanism fixed in notch position using clips

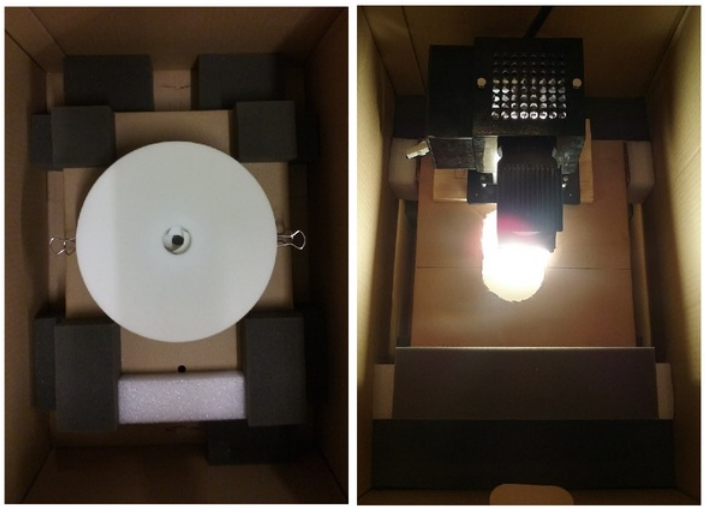

Figure 6.11: Testing set-up

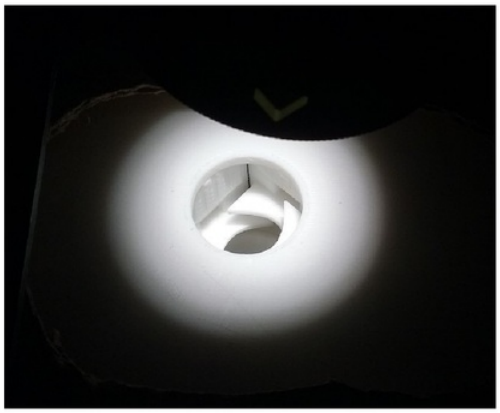

Figure 6.12: Solar simulator light shining onto receiver below aperture

Chapter 7

Results and Discussion

Analytical and experimental results are combined here in order to form the basis of the discussion. Analytical data such as the squareness (s) value and area of the aperture across the mechanism's transition from open to closed is compared to temperature data collected during testing.

7.1 Data Trends

Starting with the raw temperature data, readings were taken using a thermocouple in the mock receiver as described in section 6.2. The results for the 10A, 15A and 20A tests are shown in figure 7.1. As can be seen in figure 7.1c, for the 20A case, testing was only done for notches 4-8. The lower the notch number, the larger the aperture area and thus the higher the incident light onto the receiver. As is clear with all temperature graphs in figure 7.1, lower notch number leads to higher final temperature. Due to the prototype and receiver being made of plastic, testing was stopped at Notch 4. At this notch, a maximum temperature of 120.9°C was reached, already greater than the glass transition temperature of ABS at 104°C [47]. The glass transition temperature is the point at which the plastic starts to soften, transitioning to a more viscous state [48].

For all tests, the temperature was allowed to become relatively stable so that the approximate maximum temperatures could be determined. Looking at the results of the graphs in figure 7.1, as intuitively predicted, the lower the notch, the higher the temperature. This is consistently true for all notches and all current settings. This is promising, validating that aperture area affects temperature in the receiver. However, the relationship between notch and temperature is not the same for all currents. For example, the largest temperature difference is between Notches 4 and 5 for 10A, but 5 and 6 for 15A. This is a surprising result, but could be due to experimental errors and external factors as will be explained in section 7.2.

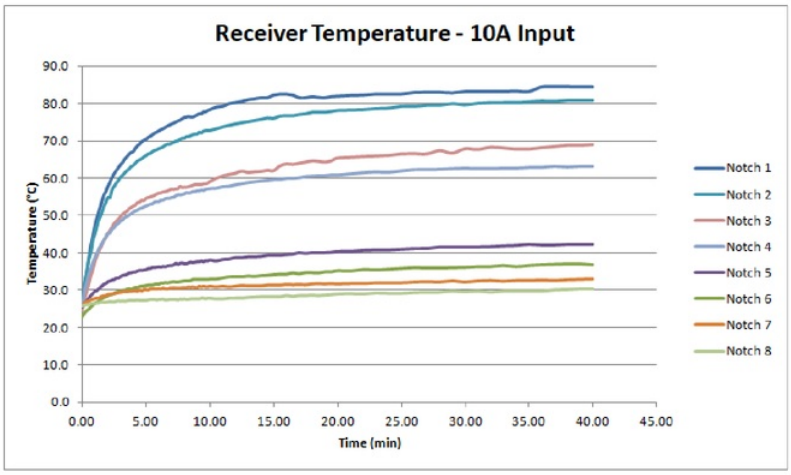

(a) 10A temperature test results

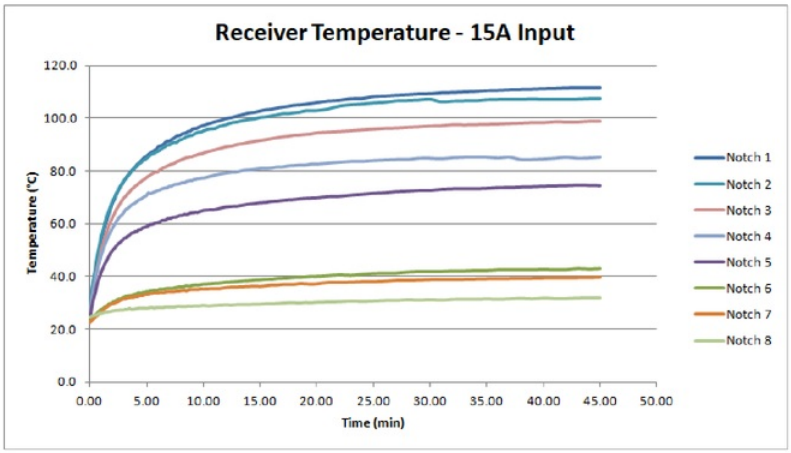

(b) 15A temperature test results

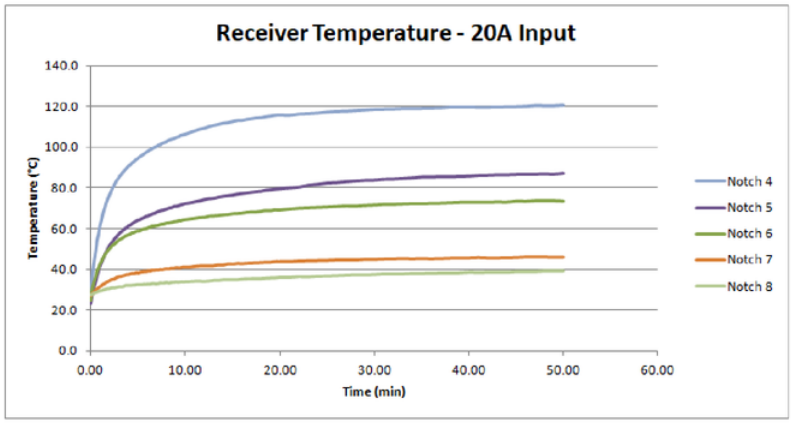

(c) 20A temperature test results

Figure 7.1: Temperature over time for notches 1-8 (10A and 15A) and 4-8 (20A)

This is demonstrated also in the graphs of figure 7.3, where the maximum temperature for each test is compared to notch (7.3a) and area (7.3b), respectively. The relationship is the same since aperture area is associated with a notch. What is interesting in this case, is that the relationship between area and maximum temperature is clearly not linear. However, it would actually be surprising if this were true, considering that not only is the area changing, but also the shape and s of the aperture, as shown in figure 5.10. As is obvious in this figure and table 5.3, the s values are not all suitable in terms of diffraction as described in Chapter 3. This will be discussed more later.

In figure 7.2, following the data lines from left to right (in order of Notch 1 to Notch 8), it is clear that while the temperature consistently goes down, the relationship with s is not linear at all. Figure 7.4 shows the relationship between maximum temperature and both amps and power density. Since current controls power density as shown in table 6.1, the graphs show the same trends. For notches 1-3, a trend cannot be established due to there being no data points from the 20A testing. Looking at Notches 4-8 however, it is clear that for most of the notches, temperature rises approximately linearly with an increase in power density. The curves for Notches 5 and 6 are not linear though, which may be due to factors to be discussed in section 7.2.

It is clear that the temperature measured in the receiver is dependent on both the squareness of the aperture shape and the area, and looking at the relationships separately does not provide a complete picture.

7.2 Sources of Error

Though using the aperture control mechanism to open and close the aperture changes the maximum temperature measured at the receiver, there are some irregularities in the data that may be due to experimental errors or external factors. As discussed in section 7.1, it would be expected that the patterns of maximum temperature and notch would be the same for all currents (fig. 7.1) but this is not the case. The same goes for the relationship between power density and maximum temperature for each notch (fig. 7.4b), with some of the curves not being linear as would be expected.

One possible cause is the variation in room temperature experienced across the tests. Though room temperature was relatively stable, it was not constant. The temperature was an average of 25.94°C, plus or minus 3.22°C. Whilst this is not a huge range, it could have still potentially influenced the results.

A possible experimental error is the misalignment between the centre of the solar simulator light source, aperture opening and receiver (see figure 6.12). Whilst it would be a small error, it is likely that some variation existed between the relative positions of these components during testing. This would affect the power density at the receiver, impacting on temperature readings. Additionally, though guards were added to the ring gear to prevent planets gears from being pulled out of place by the springs during aperture closing (fig. 6.4), there was still some movement which may have been uneven across the planet gears or inconsistent during the different rounds of testing. This would directly change the geometry of the aperture and therefore affect temperature results.

Attempts were made to make components rigid by increasing thickness and adding fillets to critical interfaces. However, due to limitations in manufacturing techniques and materials, there may have been some flexing of components, especially between cams and planet gears via the support rods between them. In section 8.2, methods of mitigating these issues will be provided so that future results may be more confidently relied upon.

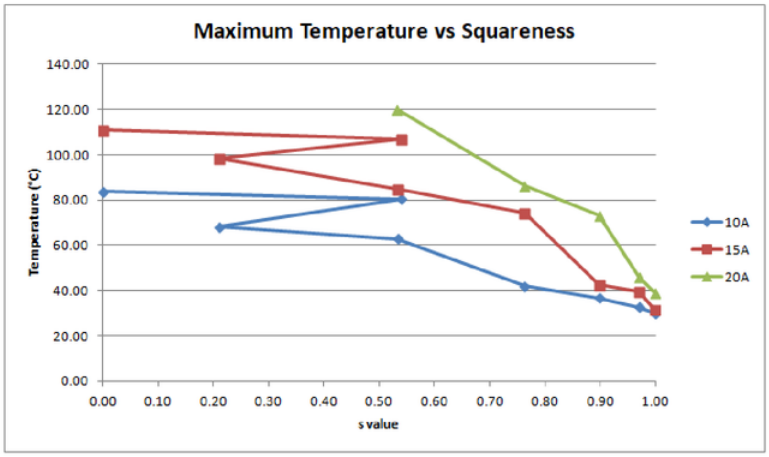

Figure 7.2: Maximum temperature versus s for 10, 15 and 20 amps

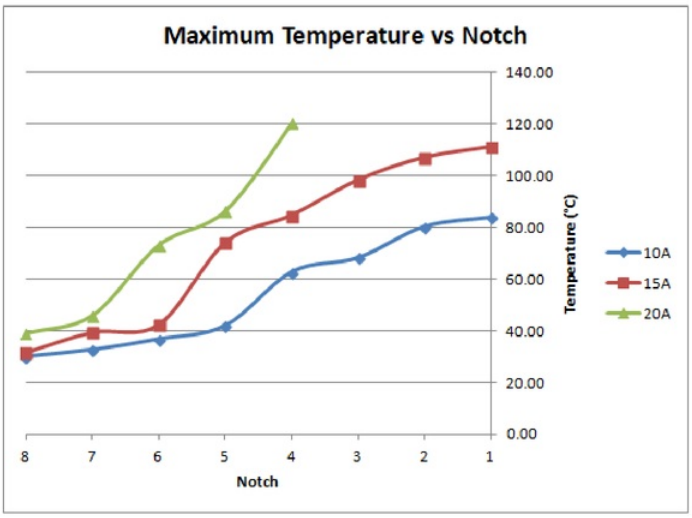

(a)

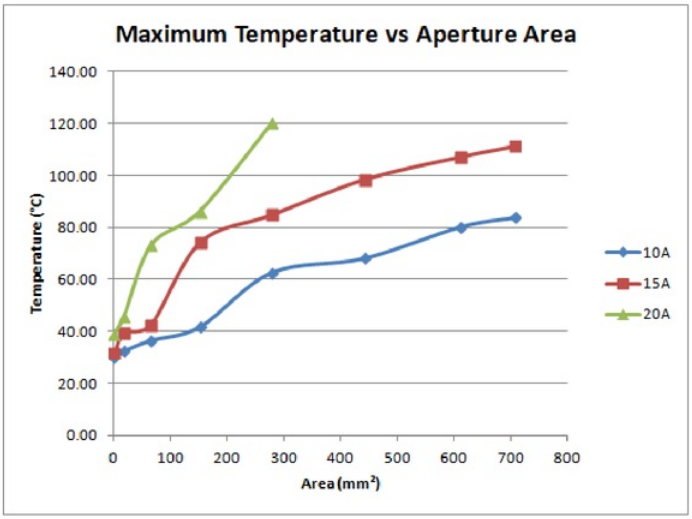

(b)

Figure 7.3: Maximum temperature versus notch (a) and aperture area (b) for 10, 15 and 20 amps

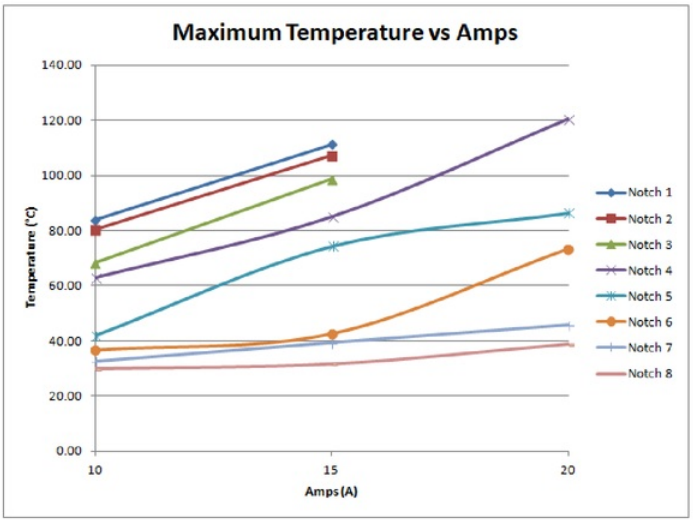

(a)

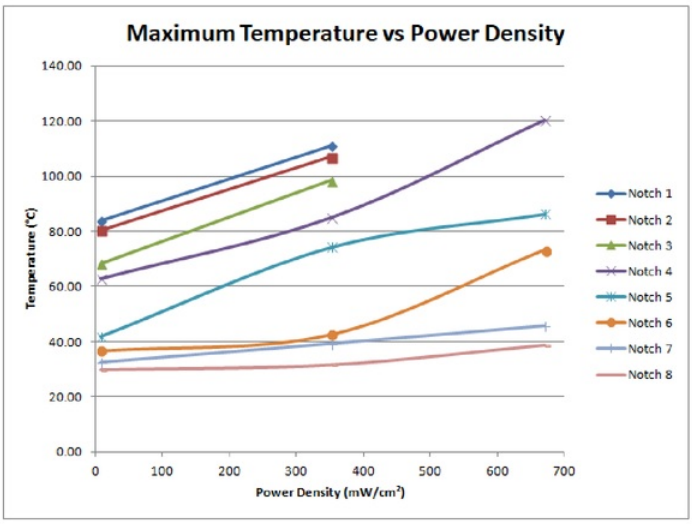

(b)

Figure 7.4: Maximum temperature versus amps (a) and power density (b) for 10, 15 and 20 amps

Chapter 8

Conclusions and Future Work

8.1 Conclusions

The problem of designing and prototyping a method of controlling temperature in a central solar thermal receiver has been solved through the work of this thesis. The solution involves an aperture control mechanism which varies the size of the receiver aperture using moving blades (followers) with a squircle profile of s=0.8. Motion of components is achieved using a planetary gear system with cams and followers.

Through the use of engineering design, modelling and both analytical and experimental data, the mechanism's ability to control temperature has been demonstrated. The success of this work means that the mechanism has the potential to work with existing concentrated solar thermal (CST) technology to bring an effective source of energy to remote communities and make existing processes more efficient with further work and future improvements.

As demonstrated through modelling and prototyping, the mechanism is functional and motion of dependent components can be controlled as intended. Temperature in the receiver has been shown to have a clear relationship to aperture properties, including area and squareness of the shape. However, examining area and squareness separately does not provide a complete picture, which is necessary in achieving more precise temperature control. Irregularities in the test results also mean that trends cannot be fully established in some cases. These irregularities may be due to experimental errors or factors relating to prototype construction or external environment during testing.

With future work, the mechanism could be made more manufacturable, automated and numerous other improvements as will be further described in section 8.2.

8.2 Future Work

The main accomplishment to be made with future work is defining the relationship between aperture area, shape and temperature. From test results, the relationship between temperature and either property in isolation is clearly not linear. Due to the combination of incident light and diffraction effects, a combined relationship must be defined before an automated system controlling the mechanism can be developed. Once defined, this relationship could be used to design the cams such that their rotation has a linear relationship to temperature. In future, a control system which reads the temperature of the receiver and adjusts the aperture based on a desired reference temperature should be designed.

As for the prototype itself, in future it should be machined out of metal. This would mean that components would be stronger, more rigid and higher temperatures for testing could be reached, more closely mimicking the environment of real life application. Tighter tolerances for components would be feasible too, reducing unwanted movement of components such as the lifting of planet gears off of their pivot points. This could also assist in the development of a more compact prototype, with unnecessary empty space eliminated. Future testing should use a more controlled set-up with less chance of variation between test runs. Testing should also be conducted in a more controlled environment with constant room temperature.

Rather than using notches in the carrier and ring gear to define aperture position, future prototypes should incorporate a stepper motor connected to the ring gear via a belt or chain. The motor would drive the ring gear and thus the followers of the aperture. In this way, finer degrees of motion could be achieved and this system could be coupled with a control system connected to the motor. In this way, it would be a completely hands-free and automated prototype.

Finally, the followers should be designed such that the s value of the aperture is less than or equal to 0.8 for as much of the cycle as possible, which could be accomplished by using sets of followers, getting increasingly smaller as the aperture is closer to being completely closed.

Chapter 9

Abbreviations

ABS	Acrylonitrile Butadiene Styrene
CAD	Computer-Aided Design
CAESAR	Catalytically Enhanced Solar Absorption Receiver
CST	Concentrated Solar Thermal
DCAR	Direct Catalytic Absorption Receiver
HTF	Heat Transfer Fluid
MEMS	Micro-electromechanical Systems
SMA	Shape Memory Alloy
STC	Solar Thermochemical Conversion

Appendix A

Meetings Attendance Form

Consultation Meetings Attendance Form

Week	Date	Comments (if applicable)	Student's Signature	Supervisor's / Co-supervisor Signature
3	15/8/17	Progress meeting + ideas discussion		
4	22/8/17	Timeline of activities + progress report expectations		
4	24/8/17	Planning of prototyping and experimentation		
6	4/9/17	Progress meeting + report discussion		
7	12/9/17	Semester break planning + experimentation discussion		
Break	28/9/17	Progress meeting + report feedback		
8	4/10/17	Testing + prototype discussion, next steps		
9	10/10/17	Prototype demonstration + testing discussion/collect		
9	13/10/17	Testing + data acquisition		
10	17/10/17	Testing progress + setup		
11	27/10/17	Report discussion + data analysis		
12	3/11/17	Data analysis + report		

Bibliography

[1] P. Palenzuela, D. C. Alarcón-Padilla, and G. Zaragoza. *Concentrating Solar Power and Desalination Plants*. Springer, 2015.

[2] M. Romero and A. Steinfeld. Concentrating solar thermal power and thermochemical fuels. *Energy Environ. Sci.*, 5:9234–9245, 2012.

[3] R. Service. Cheap catalysts turn sunlight and carbon dioxide into fuel. *Science*, June 2017.

[4] B. A. Costa and J. M. Lemos. Temperature control of a solar tower receiver based on the Lyapunov method. In *2015 23rd Mediterranean Conference on Control and Automation (MED)*, pages 583–588, June 2015.

[5] Energy technology perpectives. Technical report, International Energy Agency, 2008.

[6] *Australian Energy Resource Assessment*, chapter 10 - Solar Energy. Geoscience Australia and ABARE, 2010.

[7] E. Pihl. Concentrating solar power. *Energy Committee of the Royal Swedish Academy of Sciences*, 2009.

[8] Australian Solar Institute. *Realising the potential of Concentrating Solar Power in Australia*, 2012.

[9] L. Aichmayer. *Solar receiver design and verification for small scale polygeneration unit*. 2011.

[10] W. B. Stine and R. W. Harrigan. *Solar Energy Systems Design*. John Wiley and Sons, Inc., 1986.

[11] A. Menon and N. Ozalp. Optical analysis of variable aperture mechanism for a solar reactor. *World Acad Sci Eng Technol*, 59:925–9, 2011.

[12] S. Abdulla, H. Zahreddine, M. El Zamli, F. A. Majid, I. Rizk, Y. Al Hamidi, and N. Ozalp. Design, manufacturing and testing of a camera-like aperture mechanism for a solar reactor. In *Proceedings, ASME 2011 International Mechanical Engineering Congress and Exposition*, pages 305–319, 2011.

[13] C. Boucher. *How to Model Solar Concentrators with the Ray Optics Module*, June 2016.

[14] J. Wang, S. Yang, C. Jiang, Q. Yan, and P. D. Lund. A novel 2-stage dish concentrator with improved optical performance for concentrating solar power plants. *Renewable Energy*, 108:92–97, 2017.

[15] J. Sarwar, G. Georgakis, R. LaChance, and N. Ozalp. Description and characterization of an adjustable flux solar simulator for solar thermal, thermochemical and photovoltaic applications. *Solar Energy*, 100:179–194, 2014.

[16] A. Steinfeld and R. Palumbo. Solar thermochemical process technology. *Encyclopedia of physical science and technology*, 15(1):237–56, 2001.

[17] D. Marxer, P. Furler, M. Takacs, and A. Steinfeld. Solar thermochemical splitting of CO_2 into separate streams of CO and O_2 with high selectivity, stability, conversion, and efficiency. *Energy & Environmental Science*, 10(5):1142–1149, 2017.

[18] H. A. Najafabadi and N. Ozalp. Development of a control model to regulate temperature in a solar receiver. *Renewable Energy*, 111:95 – 104, 2017.

[19] R. Buck, J. F. Muir, and R. E. Hogan. Carbon dioxide reforming of methane in a solar volumetric receiver/reactor: the CAESAR project. *Solar Energy Materials*, 24(1-4):449–463, 1991.

[20] M. Levy, R. Levitan, H. Rosin, and R. Rubin. Solar energy storage via a closed-loop chemical heat pipe. *Solar Energy*, 50(2):179–189, 1993.

[21] A. Steinfeld, M. Brack, A. Meier, A. Weidenkaff, and D. Wuillemin. A solar chemical reactor for co-production of zinc and synthesis gas. *Energy*, 23(10):803–814, 1998.

[22] J. Petrasch, P. Osch, and A. Steinfeld. Dynamics and control of solar thermochemical reactors. *Chemical Engineering Journal*, 145(3):362–370, 2009.

[23] H. A. Najafabadi and N. Ozalp. A dynamic heat transfer model to investigate the effect of aperture size on the temperature of a solar receiver. In *Proceedings of the 8th International Symposium on Radiative Heat Transfer, RAD-16*. Middle East Technical University, 2016.

[24] L. Van den Langenbergh, C. Ophoff, and N. Ozalp. An iris mechanism driven temperature control of solar thermal reactors. In *Proceedings of the 1st Thermal and Fluid Engineering Summer Conference, TFESC*, pages 1–15. ASTFE, 2015.

[25] N. Ozalp and D. Jayakrishna. Numerical study on the thermal interaction of gas-particle transport for a vortex flow solar reactor. In *ASME 2010 4th International Conference on Energy Sustainability*, pages 133–141. American Society of Mechanical Engineers, 2010.

[26] HyperPhysics. *Circular Aperture Diffraction*, 2016.

[27] R. Kingslake. *Optics in Photography*. Press Monographs. SPIE Optical Engineering Press, 1992.

[28] Z. Ma, H. G. Merkus, and B. Scarlett. Extending laser diffraction for particle shape characterization: technical aspects and application. *Powder Technology*, 118(1):180–187, 2001.

[29] N. Ozalp, A. Toyama, M. Mohamed, M. AlShammasi, D. R. Roshan, and A. Farghaly. A smart solar reactor for environmentally clean chemical processing. *Chemical Engineering Transactions*, 25:989–994, 2011.

[30] A. Rajan, M. Abouseada, P. Manghaipathy, N. Ozalp, F. A. Majid, A. Salem, and A. Srinivasa. An experimental and analytical study on the feasibility of SMA spring driven actuation of an iris mechanism. *Applied Thermal Engineering*, 105:849–861, 2016.

[31] C. Ophoff and N. Ozalp. A novel iris mechanism for solar thermal receivers. *Journal of Solar Energy Engineering*, 139(6):061004, 2017.

[32] Photokonnexion. *Definition: Diaphragm; Iris Diaphragm; Iris*, 2017.

[33] R. A. Hill. Variable aperture collimator for high energy radiation, May 22 1984. US Patent 4,450,578.

[34] R. R. A. Syms, H. Zou, J. Stagg, and H. Veladi. Sliding-blade MEMS iris and variable optical attenuator. *Journal of micromechanics and microengineering*, 14(12):1700, 2004.

[35] M. F. Guasti. Analytic geometry of some rectilinear figures. *Int. J. Math. Educ. Sci. Technol*, 23(6):895–901, 1992.

[36] M. F. Guasti and M. C. Heredia. Diffraction pattern of a circle/square aperture. *Journal of modern Optics*, 40(6):1073–1080, 1993.

[37] C. Fong. Analytical methods for squaring the disc. *International Congress of Mathematicians*, 2014.

[38] E. W. Weisstein. Squircle. *MathWorld–A Wolfram Web Resource.*

[39] M. F. Guasti, A. M. Cobarrubias, F. J. R. Carrillo, and A. C. Rodríguez. LCD pixel shape and far-field diffraction patterns. *Optik-International Journal for Light and Electron Optics*, 116(6):265–269, 2005.

[40] R. L. Norton. *Design of Machinery: An Introduction to the Synthesis and Analysis of Mechanisms and Machines.* McGraw-Hill, 2nd edition, 1999.

[41] C. G. Cooley and R. G. Parker. A review of planetary and epicyclic gear dynamics and vibrations research. *Applied Mechanics Reviews*, 66(4):040804, 2014.

[42] Kohara Gear Industry Co.,Ltd. *Calculation of Gear Dimensions*, 2015.

[43] Kohara Gear Industry Co.,Ltd. *Basic Gear Terminology and Calculation*, 2015.

[44] R. Budynas and K. Nisbett. *Mechanical Engineering Design*. McGraw-Hill, 9 edition, 2010.

[45] E. Constans. *Analysis of Planetary Gearsets - Advanced*. Rowan University, 2013.

[46] CADQuest. *Involute Gears*, 2008.

[47] Stratasys Inc. *ABS*, 2007.

[48] Plastics differential scanning calorimetry (DSC) part 2: Determination of glass transition temperature and glass transition step height, 2013.